

Title	Structural Mechanism of Nuclear Transport Mediated by Importin and Flexible Amphiphilic Proteins
Author(s)	Yoshimura, Shige H.; Kumeta, Masahiro; Takeyasu, Kunio
Citation	Structure (2014), 22(12): 1699-1710
Issue Date	2014-11
URL	http://hdl.handle.net/2433/191327
Right	© 2014 Elsevier Ltd.
Type	Journal Article
Textversion	author

1
2
3
4
5
6
7
8
9
10
11
12
13
14
15
16
17
18
19
20
21
22
23
24
25
26
27
28
29
30
31
32
33
34
35
36
37
38
39
40
41
42
43
44
45
46
47
48
49
50
51
52
53
54
55
56
57
58
59
60
61
62
63
64
65

Title: **Structural mechanism of nuclear transport mediated by importin β
and flexible amphiphilic proteins**

Authors: Shige H. Yoshimura*, Masahiro Kumeta, and Kunio Takeyasu

Affiliations: Graduate School of Biostudies, Kyoto University

Yoshida-konoe-cho, Sakyo-ku, Kyoto 606-8501, Japan

Contact Information (corresponding author):

*Shige H. Yoshimura, Ph.D.

Graduate School of Biostudies, Kyoto University

Yoshida-konoe-cho, Sakyo-ku, Kyoto 606-8501, Japan

Tel&fax: +81-75-753-7906,

E-mail: yoshimura@lif.kyoto-u.ac.jp

Additional Footnotes: none

Running Title: Nuclear transport mediated by amphiphilic proteins

Summary

Karyopherin β family proteins mediate the nuclear/cytoplasmic transport of various proteins through the nuclear pore complex (NPC), although they are substantially larger than the size limit of the NPC. To elucidate the molecular mechanism underlying this paradoxical function, we focused on their unique structures called HEAT repeats, which consist of repetitive amphiphilic α -helices. An *In vitro* transport assay and FRAP analyses demonstrated that not only karyopherin β family proteins but also other proteins with HEAT repeats could pass through the NPC by themselves, and serve as transport mediators for their binding partners. Biochemical and spectroscopic analyses and molecular dynamics simulations of purified HEAT-rich proteins revealed that they interact with hydrophobic groups, including phenyl and alkyl groups, and undergo reversible conformational changes in tertiary structures, but not in secondary structures. These results show that conformational changes in the flexible amphiphilic motifs play a critical role in translocation through the NPC.

1 **Introduction**

2
3
4 Macromolecular trafficking between the cytoplasm and nucleoplasm is crucial for establishing proper
5
6
7 intracellular protein distributions. The nuclear pore complex (NPC), which penetrates the double
8
9
10 membrane of the nuclear envelope, controls the flow of inbound and outbound traffic. The
11
12
13 relationships between the structure and function of the NPC have been clarified by recent proteomic
14
15
16 and bioinformatics analyses (Cronshaw et al., 2002, Ori et al., 2013, Rout et al., 2000, Tamura et al.,
17
18
19 2010). The NPC is composed of more than 30 different subunits called nucleoporins (Nups). The
20
21
22 central channel is especially rich in Nups bearing Phe-Gly (FG) motifs (FG-Nups), and forms a
23
24
25 hydrophobic environment. These Nups form a hydrogel structure *in vitro* via hydrophobic
26
27
28 interactions between phenylalanine residues (Frey et al., 2006, Mohr et al., 2009).
29
30
31

32
33 Because of the macromolecular crowding, the NPC has been regarded as a molecular sieve
34
35
36 for macromolecules in the cytoplasm and nucleoplasm. Molecules smaller than 40 kDa can pass
37
38
39 through the NPC by passive diffusion, whereas proteins larger than 40 kDa cannot pass through by
40
41
42 themselves (for review, (Gorlich et al., 1999)). Numerous larger proteins are actively transported by
43
44
45 so-called transport receptors, including karyopherin β family proteins. These proteins can pass
46
47
48 through the NPC individually and can also mediate the passage of other proteins, including those
49
50
51 that are larger than 40 kDa (for review, (Chook et al., 2001)).
52
53

54
55 Important questions regarding NPC transport that remain unanswered are how transport
56
57
58 receptors mediate the translocation of the cargo in spite of their large molecular sizes, and how
59
60
61 nuclear proteins that do not interact with any known transport mediators are transported across the
62
63

1 NPC (Lange et al., 2007). A number of previous studies have demonstrated the importance of the
2
3 hydrophobic environment in the NPC for receptor-mediated nuclear transport. Karyopherin β
4
5 proteins strongly bind to hydrophobic phenyl sepharose columns (Ribbeck et al., 2002). The crystal
6
7 structure of an importin β -FG motif complex showed that importin β has several hydrophobic pockets
8
9 in its convex surface that interact with the hydrophobic residues in FG-Nups (Bayliss et al., 2000,
10
11 Bayliss et al., 2002, Liu et al., 2005, Otsuka et al., 2008). Other studies have demonstrated that a
12
13 protein's hydrophobicity is closely related to its ability to pass through the NPC (Naim et al., 2009,
14
15 Ribbeck et al., 2002). These lines of evidence imply that the size of a protein and its hydrophobicity
16
17 are critical determinants of permeability. However, the strong surface hydrophobicity and its strong
18
19 interaction with Nups cannot fully explain its rapid translocation through the NPC, because
20
21 hydrophobic proteins tend to become trapped in the NPC and cannot easily escape into the
22
23 nucleoplasm or the cytoplasm.
24
25
26
27
28
29
30
31
32
33
34
35
36
37
38

39 The crystal structures of karyopherin β family proteins exhibit significant similarity in their
40
41 overall molecular shape (Figure S1), though the primary sequence similarity is very low (15–20%
42
43 sequence identity) (O'Reilly et al., 2011, Xu et al., 2010). They are composed of a number of HEAT
44
45 motifs (19–21 repeats), each comprising two amphiphilic α -helices (A-helix and B-helix) connected
46
47 by a short linker region (Figures 1A and 1B) (Chook et al., 1999, Cingolani et al., 1999). A helical
48
49 wheel representation of the α -helices in HEAT repeats shows that the α -helices in importin β are
50
51 amphiphilic, with the hydrophobic sides facing each other toward the inside of the molecule and the
52
53 hydrophilic sides facing the outside (solvent) (Figures 1C and 1D). Due to such repetitive helices,
54
55
56
57
58
59
60
61
62
63
64
65

1 karyopherin β has large structural flexibility, which has been demonstrated to play important roles
2
3
4 in binding to cargo proteins and RanGTP (Chook et al., 2001, Conti et al., 2006, Forwood et al., 2010,
5
6
7 Lee et al., 2000, Stewart, 2007).
8
9

10 In this report, we focused on the structural flexibility of karyopherin β and other HEAT
11
12 motif-rich proteins, and examined their involvements in passage through the NPC. The flexible
13
14 structure with amphiphilic α -helices seems suitable for passing through the hydrophobic crowding
15
16 environment of the NPC, and travel between the cytoplasm and the nucleoplasm. Therefore,
17
18
19 conformational changes that occur in such a flexible amphiphilic structure play a critical role not only
20
21
22 in interaction with cargo but also in fast passage through the NPC. Our extensive functional and
23
24
25 structural analyses revealed that importin β and other HEAT motif-rich proteins undergo
26
27
28 conformational changes induced by various hydrophobic groups.
29
30
31
32
33
34
35
36
37
38
39
40
41
42
43
44
45
46
47
48
49
50
51
52
53
54
55
56
57
58
59
60
61
62
63
64
65

Results

The HEAT motif is a suitable structure for passage through the NPC

Non-karyopherin β family member proteins which contain multiple HEAT motifs are listed in Figure 2A. The number of HEAT motifs and their positions within the polypeptide vary from protein to protein. Since the primary sequence similarity of HEAT motif is very low, we also examined their secondary structures (amphiphilic α -helices, Figure 1C) and found additional possible HEAT motifs within the molecule (see Supplemental Experimental Procedures for detail). The results are summarized in Figure 2A. We expressed these HEAT-rich proteins in bacterial cells either as full-length proteins or as partial fragments containing HEAT-rich regions, purified them by affinity chromatography, and subjected them to circular dichroism (CD) spectra analysis. All the HEAT-rich fragments showed typical α -helix-rich spectra (Figure S2A) and high α -helical content comparable to that of importin β (Figure S2B).

We then tested whether these HEAT-rich fragments could travel through the NPC. EGFP-fused HEAT-rich proteins, and non-HEAT proteins as controls, were expressed in bacteria, affinity purified, and incubated with digitonin-treated HeLa cells. As shown in Figure 2B, HEAT-rich proteins were able to enter the nucleus through the NPC without the assistance of other proteins. This influx is not due to the EGFP tag, as we observed similar results with HA-tagged proteins that were immunostained with an anti-HA antibody (Figure S2C). It should be noted that all of these HEAT-rich proteins are far larger than the size limit of the NPC (~ 40 kDa). The flux rate constant was plotted against the size of the protein (Figure 2C) (The Stokes radius was obtained by gel

1 filtration chromatography as described in Figure S2D). The flux rates of non-HEAT proteins were
2
3
4 drastically reduced above a Stokes radius of 4 nm. In contrast, all of the HEAT-rich proteins showed
5
6
7 high flux rates, indicating that they can overcome the size barrier of the NPC regardless of
8
9
10 molecular size. The influx of HEAT-rich proteins was almost completely blocked by wheat germ
11
12
13 agglutinin (Figure 2B, +WGA), which indicated that they indeed traveled through the NPC. The
14
15
16 pull-down assay also demonstrated direct interactions between HEAT-rich proteins and
17
18
19 nucleoporins (Figure 2D), confirming that HEAT-rich proteins interact with Nups when they go
20
21
22 through the pore.
23

24
25
26 The intracellular distribution and dynamics of the HEAT-rich proteins were also examined by
27
28
29 expressing EGFP-fusion proteins in HeLa cells. The steady-state distributions varied from protein
30
31
32 to protein; some proteins strongly accumulated in the nucleus, whereas others were less in the
33
34
35 nucleus and mainly located in the cytoplasm (Figure 3, and summarized in Figure 2A). The proteins
36
37
38 that showed strong nuclear signals were then subjected to FRAP analysis to examine their
39
40
41 steady-state shuttling across the nuclear envelope. The analysis of fluorescence recovery
42
43
44 demonstrated that these proteins shuttle between the nucleoplasm and the cytoplasm (Figure 3). The
45
46
47 flux rates obtained *in vivo* (FRAP analysis, Figure 3) were in general smaller than those *in vitro*
48
49
50 (transport assay, Figure 2B), suggesting that these HEAT-rich proteins may form a complex *in vivo*
51
52
53 and may regulate shuttling of the protein complex through the NPC.
54
55
56
57
58
59
60

61 ***HEAT-rich proteins mediate the translocation of other proteins through the NPC***
62
63

1 We then examined whether HEAT-rich proteins assist the nuclear transport of other proteins and act
2
3
4 as potential transport mediators. CAND1 (~120 kDa) contains 27 HEAT repeats and is known to
5
6
7 form a complex with cullin1 and cullin4B (Fischer et al., 2011, Goldenberg et al., 2004) (Figures
8
9
10 4A and 4B). Purified cullin4B was excluded from the nucleus of permeabilized HeLa cells, but was
11
12
13 able to enter the nucleus when it formed a complex with CAND1 (Figure 4C), demonstrating that
14
15
16 CAND1 stimulates the influx of cullin4B despite the increase in total molecular mass. We
17
18
19 confirmed this function *in vivo* by measuring the mobility of EGFP-fused cullin across the nuclear
20
21
22 envelope in CAND1-knockdown cells (Figure 4D). As demonstrated by the FRAP analysis,
23
24
25 fluorescence recovery in the nucleus was drastically reduced by the depletion of CAND1 (Figure
26
27
28 4E). In particular, the recovery of cullin4B was significantly reduced in CAND1-knockdown cells.
29
30
31 The shuttling of cullin1 in control cells was slower than that of cullin4B, but was also significantly
32
33
34 reduced by knockdown of CAND1.
35
36
37
38

39 The same effect was observed for the protein phosphatase 2A (PP2A) complex, in which the
40
41
42 HEAT-rich subunit (A subunit), the catalytic subunit (C subunit), and the regulatory subunit (B
43
44
45 subunit) form a trimeric complex (Figure 5A) (Cho et al., 2007). HeLa cells express two isoforms
46
47
48 of the A subunit (PPP2R1A (A α) and PPP2R1B (A β)). When the EGFP-fused C subunit was
49
50
51 expressed in HeLa cells, it localized to both the cytoplasm and nucleoplasm. Bleaching of the
52
53
54 nuclear fluorescent signal resulted in fast recovery of the signal (Figures 5B and 5C). Knockdown
55
56
57 of the HEAT subunit (Figure 5D) reduced the flux rate of the EGFP-fused C subunit across the
58
59
60 nuclear envelope (PPP2R1A KD and PPP2R1B KD, Figures 5B and 5C). These results
61
62
63
64
65

1 demonstrated that some HEAT-rich proteins can not only pass through the pore, but also could assist
2
3
4 the passage of other proteins. Since a previous report demonstrated direct interaction between
5
6
7 PPP2R1A and importin 9 (Lubert et al., 2003), we also tested the involvement of importin 9 in the
8
9
10 nuclear shuttling of PP2A. Knockdown of importin 9 only slightly decreased the mobility of the
11
12
13 PP2A C subunit, while double-knockdown of importin 9 and PPP2R1A resulted in a further
14
15
16 decrease of the recovery (Figure S3). This result indicates that the PP2A A subunit is a major
17
18
19 transport mediator of the PP2A complex and importin 9 may have additional regulatory roles in the
20
21
22 intracellular distribution of the enzyme (see Discussion).
23
24
25
26
27
28

29 ***HEAT-rich proteins bind to hydrophobic groups and undergo conformational changes***

30
31
32 The central channel of the NPC is protein-rich environment with high content of hydrophobic
33
34
35 residues; the pore-forming Nups contain a number of phenylalanine and leucine, as well as high
36
37
38 numbers of non-bulky side chains such as serine, threonine, and glycine (Figure S4A). In addition,
39
40
41 significant portions of these Nups are assigned as unstructured (Figure S4B) and do not show any
42
43
44 significant secondary structures based on the CD spectra (Figure S4C) (Denning et al., 2003). The
45
46
47 interaction between HEAT-rich proteins and various hydrophobic groups were investigated by
48
49
50 hydrophobic interaction chromatography. As shown in Figure 6A, purified HEAT-rich proteins
51
52
53 firmly bind not only to phenyl sepharose, as was demonstrated for importin β in previous studies
54
55
56 (Ribbeck et al., 2002), but also to other alkyl groups such as butyl (C4) and octyl (C8). This result
57
58
59 well matches to the pull-down assay between HEAT-rich proteins and FG-rich domain of
60
61
62
63
64
65

1 nucleoporin (Figure 2D). Increasing the salt concentration strengthened the binding (Figure 6A,
2
3
4 NaCl⁺), demonstrating that the interaction is mainly governed by hydrophobic interactions.
5
6

7 Since HEAT motifs are composed of amphiphilic helices (Figure 1), we tested whether
8
9
10 hydrophobic groups can induce conformational changes of HEAT motifs. The tertiary structure of
11
12 purified HEAT-rich proteins in various organic solvents was investigated by examining the
13
14 fluorescence spectra of internal tryptophan residues. As summarized in Figure 6B, the center of the
15
16 fluorescence spectra of internal tryptophan residues. As summarized in Figure 6B, the center of the
17
18 fluorescence peak was more or less red-shifted as the alcohol concentration increased, implying that
19
20 the residue is exposed to the solvent. The size of the shift largely depended on the alkyl species; as
21
22 the alkyl chain became longer, the effect became stronger (Figure 6B), indicating that the
23
24 conformational change was induced by an alkyl group, and not by a hydroxyl group. The details of
25
26 conformational flexibility was further investigated by mutating tryptophan residues in importin β .
27
28
29 As summarized in Figure S4D, structural changes were more prominent in the middle regions
30
31 (HEAT #7-11) than those in both termini (HEAT #1-4 and #19). It should also be noted that these
32
33 structural changes are reversible, since HEAT-rich proteins, which was once exposed to 50 %
34
35 alcohol and then placed back to alcohol-free solution exhibited the tertiary structure similar to the
36
37 non-treated protein (Figure S4E).
38
39
40
41
42
43
44
45
46
47
48
49
50

51 In contrast to the tertiary structures, the secondary structures were not affected by the
52
53 hydrophobic groups. The CD spectra of HEAT-rich proteins showed a typical α -helix-rich shape in
54
55 the absence and presence of hydrophobic groups (Figure S4F). The molar ellipticity at 222 nm,
56
57 which corresponds to an α -helix-specific negative peak, was summarized in Figure 6C. The
58
59
60
61
62
63
64
65

1 α -helical contents of HEAT-rich proteins were not reduced in the presence of high concentrations of
2
3
4 hydrophobic groups and rather slightly increased due to the stabilizing effect of alcohol.
5
6
7
8
9

10 ***Structural flexibility is required for translocation through the NPC***

11
12
13 The importance of structural flexibility was examined in an *in vitro* transport assay. Purified
14
15
16 HEAT-rich proteins were fixed by a crosslinker (BS³) to restrict conformational flexibility. The
17
18
19 fixed proteins showed almost the same elution profile as non-treated proteins in gel filtration
20
21
22 chromatography, but less structural dynamics upon exposure to the hydrophobic groups (Figures
23
24
25 S5A and S5B). These prefixed HEAT-rich proteins showed a slower influx rate in the *in vitro*
26
27
28 transport assay (Figure 7, crosslinked), indicating that structural flexibility plays a critical role in
29
30
31 traveling through the NPC. This effect was not due to the modification of side chains by the
32
33
34 crosslinker, since the same modification without crosslinking did not significantly affect the flux
35
36
37 rate (Figure 7, non-crosslinked). These results indicate that structural flexibility plays a critical role
38
39
40 in translocation through the NPC.
41
42
43
44
45
46
47

48 ***Molecular dynamics simulation of conformational changes***

49
50
51 The molecular dynamics (MD) simulation of the structural changes occurring in importin β
52
53
54 correlated well with the experimental results (Figure 6) and provided more detailed structural
55
56
57 information. The MD simulation was initiated from the previously reported crystal structure for
58
59
60 mouse importin β (Protein Data Bank ID: 1UKL) (Figure S1), and was executed in two different
61
62
63
64
65

1 solvents (water or 50% (v/v) TFE/water mixture) until the structure became stable (Figure S6A). As
2
3
4 shown in Figures 8A and 8B, and as quantified in Figures 8C and 8D, most of the α -helices in the
5
6
7 HEAT motifs remained unchanged, although occasional and partial elongations were detected in
8
9
10 50% TFE (Figure 8D). The structural fluctuation is even smaller in 50% TFE than in water (the root
11
12
13 mean square fluctuation was 0.714 in 50% TFE and 0.948 in water). This result is in accordance
14
15
16 with the results from the CD spectra (Figure 6), and it indicates that most of the secondary structure
17
18
19 is retained (in fact, it is even more stabilized) in the water/alcohol mixture.
20
21
22

23 In contrast to the secondary structure, the interactions among adjacent helices are significantly
24
25
26 affected by the environment. As shown in Figures 8A and 8B, and quantified in Figures 8E and 8F,
27
28
29 the distances between adjacent α -helices were increased. Changes in the carboxyl terminal half
30
31
32 were particularly prominent (Figure 8F). The collapse in tertiary structure was also observed in
33
34
35 other trajectories in TFE, although the position and timing varied from trajectory to trajectory
36
37
38 (Figure S5B). The dissociation of adjacent helices is as expected, since hydrophobic interaction
39
40
41 generally becomes weaker in a hydrophobic environment. This separation of α -helices resulted in
42
43
44 the exposure of hydrophobic side chains to the molecular surface (Figure 8G–I). The
45
46
47 solvent-excluded surface area (SESA) assigned to the hydrophobic residues was 1.7 times larger in
48
49
50 50% TFE than in water (Figure 8I). In 50% TFE, the first hydration shell was severely collapsed
51
52
53 and the TFE molecules were in close contact with hydrophobic residues at the protein surface
54
55
56 (Figure S5F), indicating that hydration energy is closely related to the conformational change of
57
58
59 importin β . TFE attacks hydrophobic surface regions including the previously identified binding
60
61
62
63
64
65

1 pockets for the FG motif (Bayliss et al., 2000, Bayliss et al., 2002, Bednenko et al., 2003) and
2
3
4 induces separation of the HEAT helices.
5
6

7 The reversibility of the solvent-induced conformational changes could also be seen in the MD
8
9 simulation. Transferring importin β from 50% TFE to water resulted in an immediate decrease in
10
11 the hydrophobic surface area; the hydrophobic SESA of importin β increased when exposed to TFE,
12
13 but rapidly returned to its initial level when transferred to water (at 100 or 200 ns; Figure 8J). These
14
15 results are consistent with the experimental observation that the solvent-induced conformational
16
17 changes of importin β are reversible (Figure S4E).
18
19
20
21
22
23
24
25
26
27
28

29 ***Importin β -cargo complex also undergoes conformational change***

30
31 Structural changes in importin β loaded with a cargo (importin β -binding (IBB) domain of importin
32
33 α) were also characterized (Figure 9). A pull-down assay demonstrated that the IBB domain did not
34
35 dissociate from importin β even in the presence of 50% TFE (Figure 9A), which is reasonable since
36
37 the interaction between importin β and IBB is mainly governed by electrostatic interactions
38
39 (Cingolani et al., 1999). The effect of TFE on the CD spectrum of the entire complex was similar to
40
41 that of free importin β : low concentrations (10–30%) of TFE did not affect the α -helix content,
42
43 whereas higher concentrations slightly increased the α -helix content (Figure 9B, red). The
44
45 fluorescence spectrum suggested that the tertiary structure of the complex was significantly affected
46
47 by low concentrations of TFE (Figure 9B, blue), although the effect was slightly smaller than that
48
49 observed with free importin β (compare with Figure 6B), suggesting that the IBB domain helps
50
51
52
53
54
55
56
57
58
59
60
61
62
63
64
65

1 stabilize the tertiary structure of importin β (Cingolani et al., 2000).
2
3

4 MD simulation of the importin β -IBB complex was performed using the previously reported
5
6 crystal structure (PDB ID: 1QGK; Figure S1) as the starting structure. Interactions between
7
8 importin β and the IBB domain in 50% TFE were retained throughout our simulation time (400 ns;
9
10 Figures 9C and 9D; see also Figure S5D), which is in agreement with the pull-down experimental
11
12 results (Figure 9A). As observed with free importin β , the HEAT-HEAT distances (Figures 9E and
13
14 9F) and hydrophobic SESA (Figures 8I, 9G and 9H) significantly increased in the presence of TFE,
15
16 whereas the length of each α -helix remained unaffected in both cases (Figure S6E). The pattern of
17
18 the increase in distance (Figure 9F) slightly differed from that of free importin β (Figure 8F), in part
19
20 due to the interaction of importin β with IBB via its carboxyl terminal HEAT domains (Cingolani et
21
22 al., 1999). These results demonstrate that the importin β -IBB complex undergoes conformational
23
24 changes similar to those of free importin β , although the changes in the entire conformation are
25
26 slightly smaller due to the interaction with the IBB domain.
27
28
29
30
31
32
33
34
35
36
37
38
39
40
41
42
43
44

45 **Discussion**

46
47 It has long been known that the NPC restricts the flow of molecules based mainly on their size and
48
49 shape. Smaller molecules can pass through the NPC, whereas larger molecules cannot. However,
50
51 such larger proteins can be translocated through the NPC with the aid of transport receptors. The
52
53 unresolved questions about NPC and transport mediators are i) how importin β family proteins pass
54
55 through the NPC despite their large molecular size, and ii) whether more than 1,000 nuclear
56
57
58
59
60
61
62
63
64
65

1 proteins are imported by only dozens of known transport receptors. In this study, we focused on the
2
3 flexible amphiphilic structure of importin β and other HEAT motif-rich proteins, and clearly
4
5 demonstrated that not only importin β but also other HEAT motif-rich proteins can pass through the
6
7 NPC by themselves and, in some cases, together with cargo. Our findings provide an answer to the
8
9 size-barrier paradox of receptor-mediated nuclear transport, propose one general structural property
10
11 of “transport receptors”, and suggest the existence of numerous cargo-specific transport receptors
12
13 and “transport-regulating subunits”.
14
15
16
17
18
19
20
21
22
23
24
25

26 *Amphiphilic motifs are suitable for passage through the NPC*

27

28
29 Our results shown in Figures 2 and 3 demonstrated that not only importin β but also many other
30
31 proteins that contain a number of HEAT motifs can pass through the NPC. All of the proteins we
32
33 investigated are larger than 40 kDa and, therefore, exceed the “size barrier” of the NPC. There have
34
35 been several previous reports that demonstrated importin β -independent nuclear translocation of
36
37 over-sized proteins. These include albumin (66 kDa) with hydrophobic modifications on the surface
38
39 (Naim et al., 2009, Ribbeck et al., 2002), amphiphilic triple-helix of spectrin repeat (Kumeta et al.,
40
41 2012), and importin α and β -catenin, both of which contain amphiphilic helical repeats similar to
42
43 HEAT repeats (ARM repeats) (Fagotto et al., 1998, Koike et al., 2004, Wiechens et al., 2001). These
44
45 lines of evidence strongly suggest that hydrophobic/hydrophilic property of the protein is closely
46
47 related to its passage through the NPC. The protein structure database contains a number of proteins
48
49 with repetitive amphiphilic α -helical motifs in addition of the HEAT motif (D'Andrea et al., 2003,
50
51
52
53
54
55
56
57
58
59
60
61
62
63
64
65

1 Groves et al., 1999, Marsella et al., 2009, Neuwald et al., 2000). Although the detailed arrangements
2
3
4 of helices (and sheets) vary from motif to motif, they are structurally flexible and involved in
5
6
7 interaction with other proteins (Bella et al., 2008, Neuwald et al., 2000, Shi, 2009). Therefore, it
8
9
10 might be the case that not only HEAT-rich proteins, but also proteins with repetitive amphiphilic
11
12
13 motifs might translocate through the NPC.
14
15

16 We further demonstrated that non-karyopherin HEAT-rich proteins, CAND1 and PPP2R1,
17
18
19 function as specific nuclear transport receptors for their binding partners (Figures 4 and 5). These
20
21
22 proteins have been identified as a component of multi-subunit protein complexes, but not as a
23
24
25 transport receptor. PPP2R1 is one of the three subunits of protein phosphatase 2A (PP2A) complex
26
27
28 and has been regarded as a scaffolding subunit (A subunit) which directly interacts with both of the
29
30
31 other two subunits (B and C subunits) (Figure 5A). PP2A is highly conserved from yeast to human
32
33
34 and is known to dephosphorylate a number of cellular proteins (Janssens et al., 2008, Shi, 2009). The
35
36
37 regulatory mechanism of PP2A is extraordinarily complex because of the existence of multiple
38
39
40 isoforms in each subunit; 2 isoforms (A α and A β) for A subunit, 2 isoforms (C α and C β) for C
41
42
43 subunit, and at least 19 isoforms for B subunit (Janssens et al., 2008). Especially, the B subunit
44
45
46 affects the substrate specificity and the catalytic activity of the holoenzyme. On the other hand, the
47
48
49 function of the HEAT-rich A subunit has not been well understood, except that it functions as a
50
51
52 flexible scaffold. Our result presented here demonstrated that the A subunit plays a role in the
53
54
55 translocation of the holocomplex through the NPC. Considering the fact that the B subunit also has
56
57
58
59
60
61
62
63
64
65

1 a HEAT-like structure (Figure 5A, blue) (Cho et al., 2007), both A and B subunits may regulate the
2
3
4 intracellular localization of the enzyme.
5
6

7 Double-knockdown of importin 9 and the A subunit resulted in a further decrease of the
8
9
10 flux rate of the C subunit (Figure S3). This implies that both importin 9 and the HEAT-rich subunit
11
12
13 are involved in nuclear shuttling. It might be the case that PPP2R1A confers a constitutive
14
15
16 permeability to the holoenzyme, while importin 9 plays more regulatory roles in the intracellular
17
18
19 distribution of the complex. It is intriguing that PP2A directly interacts with HDAC4 and
20
21
22 dephosphorylates it, which results in the nuclear import of HDAC4 (Paroni et al., 2008). Since
23
24
25
26 PP2A is shuttling between cytoplasm and nucleoplasm, it might be the case that PP2A regulates the
27
28
29 intracellular localization of various substrates by converting phosphorylated and dephosphorylated
30
31
32 states. Our result on PPP4R1 (Figures 2 and 3), which is a regulatory subunit of protein phosphatase
33
34
35 4 (PP4), suggests that the intracellular distribution of PP4 is also regulated by this HEAT-rich
36
37
38 subunit. Therefore, one of the important functions of HEAT-rich and other amphiphilic proteins in a
39
40
41 protein complex might be regulating the intracellular distribution of the complex in a karyopherin
42
43
44 β -independent manner.
45
46
47
48
49
50

51 ***Conformational changes in HEAT-rich proteins in hydrophobic environment***

52

53
54
55 Our structural analysis on importin β and other HEAT-rich proteins demonstrated that reversible
56
57
58 conformational change is critical in traveling through hydrophobic crowding of the NPC (Figures 6
59
60
61 and 7). Although a direct interaction between Nups and transport receptors has been reported in
62
63
64
65

1 previous studies, a simple binding event cannot explain the passage mechanism because strong
2
3
4 binding to Nups results in a longer residence time in the NPC and poor escape to the opposite side.
5
6
7 Repetitive amphiphilic structures and their flexible and reversible conformational changes could
8
9
10 clearly explain the mechanism of such fast passage. The structural flexibility of karyopherins has
11
12
13 been reported and discussed in previous studies, mainly based on the crystal structures of
14
15
16 karyopherins bound with cargo, RanGTP or FG-Nups (Chook et al., 2001, Conti et al., 2006,
17
18
19 Forwood et al., 2010, Lee et al., 2000, Stewart, 2007). The interaction with RanGTP and some of
20
21
22 the cargos mainly occurs at the concave surface (B-helices) of importin, whereas interaction with
23
24
25 FG-motifs (FG-Nups) and some of the cargo occur at the convex surface. Our results (Figure 6B,
26
27
28 S4D, 8 and 9) suggest that Nup-induced conformational changes of importin β occur over a wide
29
30
31 area of the molecule, especially in the middle HEAT repeats (#5-17). Repetitive alignment of A-
32
33
34 and B-helices on the opposite sides of the molecule (A-helix on the convex and B-helix on the
35
36
37 concave) and their flexible conformation enables HEAT proteins to interact both with the cargo and
38
39
40 nucleoporins without affecting each other, which plays a critical role in efficient passage through
41
42
43 the NPC as a protein complex.
44
45
46

47
48 Our result shown in Figure 6 indicates that conformational changes in HEAT motifs are
49
50
51 induced by interaction with various kinds of hydrophobic groups (ethyl, butyl, propyl, octyl, and
52
53
54 phenyl). This type of conformational change is in clear contrast to ligand-dependent conformational
55
56
57 changes, which are mediated by specific interactions between the ligand and specific residues in the
58
59
60 target enzyme. In the case of importin β , our MD simulation revealed a number of weak interactions
61
62
63

1 between hydrophobic groups in the solvent and many hydrophobic side chains (Figure S6F). Such
2
3
4 weak interaction between importin β and hydrophobic groups of Nups plays an important role in the
5
6
7 fast kinetics of the translocation process, which had been observed in previous reports using bulk
8
9
10 import assay and single-molecule observation (several tens of milliseconds) (Sun et al., 2008, Tu et
11
12
13 al., 2011). In good agreement with this is the transport ability of importin β which lacks FG-binding
14
15
16 pocket(s). Importin β contains multiple binding pockets for FG-motifs (Bayliss et al., 2000,
17
18
19 Bednenko et al., 2003). However, mutating these critical amino acids could not completely abolish
20
21
22 the transport ability (Figure S7), suggesting that the interaction between importin β and
23
24
25 nucleoporins is not of a site-specific manner. Dissociation rate constant (k_{off}) between importin β
26
27
28 and FG-Nups obtained in *in vitro* binding assay (10^{-3} – 10^{-4} ·sec⁻¹) does not explain such fast kinetics,
29
30
31 since hydrophobic interaction *in vitro* condition is extremely stronger than that in the hydrophobic
32
33
34 environment of the NPC.
35
36
37
38
39
40
41
42
43
44

45 ***Molecular Events within the NPC***

46
47
48

49 Although HEAT-rich proteins can mediate translocation of the cargo, karyopherin β family proteins
50
51
52 are distinct from others because they can catch or release cargo depending on the RanGTP/GDP
53
54
55 cycle. Importin β releases the cargo when bound to RanGTP, which is rich in the nucleoplasm
56
57
58 (Figure 10A). Due to this mechanism, importin and exportin can produce a cargo gradient across
59
60
61
62
63
64
65

1 the nuclear envelope (Gorlich et al., 2003), even though their passage through the NPC itself is
2
3
4 bi-directional and energy-independent. In contrast to karyopherin β proteins, other HEAT-rich
5
6
7 proteins do not actively produce a cargo gradient across the nuclear envelope, because their passage
8
9
10 through the NPC is mainly diffusion-based (Figure 2B), and their interaction with the cargo is
11
12
13 Ran-independent (Figure 4B). In good agreement with this is the previous reports that ARM repeat
14
15
16 proteins can mediate the nuclear import of other proteins (CaMKIV by importin α (Kotera et al.,
17
18
19 2005) and lef-1 by β -catenin (Asally et al., 2005)) but do not produce a strong accumulation of the
20
21
22 cargo in the nucleus (Yokoya et al., 1999). Although non-karyopherin β HEAT-rich proteins cannot
23
24
25 produce the cargo gradient in Ran-dependent manner, they might have other regulatory mechanisms
26
27
28 on cargo-release.
29
30

31
32
33 The possible molecular events that occur during the passage of an amphiphilic protein
34
35
36 through the NPC are depicted in Figure 10B. When an amphiphilic protein or protein complex
37
38
39 enters the NPC from the cytoplasmic side, it may initially bind to part of the NPC with some
40
41
42 structural and positional fluctuations. Nup358 (RanBP2) may help capture and anchor karyopherin
43
44
45 β to the cytoplasmic side of the NPC. The protein eventually moves into the central channel by
46
47
48 repeated interaction with hydrophobic groups, or in some cases, it escapes back into the cytoplasm.
49
50
51 Once inside the central pore of the NPC, the protein travels in the pore by diffusion. As the
52
53
54 interactions between the hydrophobic surface of the protein and FG-Nups are very weak in a
55
56
57 hydrophobic environment, the diffusion rate becomes much higher than that obtained *in vitro*. At a
58
59
60
61
62
63
64
65

1 certain point during diffusion, the protein reaches the nucleoplasmic border of the NPC, and
2
3
4 occasionally dissociates from the NPC.
5
6

7
8 The detailed structural information of the central channel of the NPC will lead further
9
10 understanding of the molecular event of protein passage. Long-term MD simulation (as described
11
12 by (Isgro et al., 2005)) including such structural information will also provide useful information on
13
14 the dynamics of molecular crowding (water, polar groups, and hydrophobic groups) within the NPC,
15
16
17 and on the contribution of amphiphilic motifs in migrating through such a crowding environment.
18
19
20
21
22
23
24
25
26
27
28
29
30
31
32
33
34
35
36
37
38
39
40
41
42
43
44
45
46
47
48
49
50
51
52
53
54
55
56
57
58
59
60
61
62
63
64
65

1 **Experimental Procedures**

2 3 4 **DNA construction and protein purification**

5
6
7 GST-tagged mouse importin β was expressed in bacterial cells and purified as described in a
8
9
10 previous study (Bayliss et al., 2000, Bayliss et al., 2002, Liu et al., 2005, Otsuka et al., 2008). The
11
12
13 cDNAs encoding human HEAT-rich proteins and non-HEAT proteins were either cloned by PCR
14
15
16 from a cDNA pool of HeLa cells (PPP2R1A, PPP2R1B, PPP4R1, CAPG), or purchased from the
17
18
19 Kazusa DNA library. cDNA fragments of HEAT-rich regions and the fragments of cullin were
20
21
22 amplified by PCR and subcloned into the pGEX vector (GE Healthcare). The proteins were
23
24
25 expressed as GST-fusion proteins and were subjected to specific protease digestion (PreScission; GE
26
27
28 Healthcare) or thrombin (Nacalai Tesque) if necessary. The cDNA fragment encoding the importin
29
30
31 β -binding domain of rat importin α (IBB; a.a. 1–69) was amplified by PCR from full-length cDNA
32
33
34 and cloned into a pET29 vector (Novagen). The protein was expressed in *E. coli* and purified by
35
36
37 ion-exchange chromatography (Hi-Trap SP; GE Healthcare) followed by gel filtration
38
39
40 chromatography (Superdex 75; GE Healthcare).
41
42
43
44

45 **Protein fixation**

46
47
48 Purified importin β was diluted into different solvents (0 or 50% TFE with 50 mM KPO₄) to a final
49
50
51 concentration of 2 mg/mL. A bifunctional crosslinker (BS³; Thermo Science) or sulfo-NHS
52
53
54 (Thermo Science) was added at a final concentration of 1 mM, and the mixture was incubated at 25
55
56
57 °C for 30 min. The reaction mixture was then subjected to a gel filtration column to replace the
58
59
60 buffer with 100 mM KPO₄.
61
62
63
64
65

CD and fluorescence spectra

The CD spectra of purified karyopherins and other HEAT proteins were measured using a J-805 (JASCO) with a 0.1-cm cuvette. Data was acquired every 0.1 nm between 200 and 250 nm.

Fluorescence spectra of purified importin β (1 μ M) and free N-acetyl tryptophan (8 μ M) were measured using a fluorometer FP-8200 (JASCO) with a 3 mm \times 3 mm cuvette. Samples were dissolved in 50 mM of KPO_4 (pH 7.4) with various concentrations of organic solvents (0–50%).

The difference of the peak center wavelength between importin β and free N-acetyl tryptophan was calculated at each solvent condition.

Molecular dynamics simulations

The MD simulations were conducted using the Amber11 package with an ff99SB force field. TFE parameters were set by a general AMBER force field. A GPU version of the particle mesh Ewald method was used with an NVIDIA Tesla M2090. The time step was 2 fsec, a constant 310 K temperature was maintained using Langevin dynamics with a collision frequency of 1.0 psec⁻¹, and the pressure was kept at 1 atm with a relaxation time of 2.0 ps. Bonds involving hydrogen atoms were constrained using the SHAKE algorithm, and the long-range interaction cut-off was set to 15.0 Å.

FRAP analysis

EGFP-fused HEAT-rich proteins were expressed in HeLa cells cultured in DMEM supplemented with 10% FCS. The microscopic observations were performed using confocal laser scanning microscope system (FV1200, Olympus), equipped with a stage chamber (Tokai Hit). The nucleus

1 was bleached by a 488 nm laser at maximum output for 5 sec. After bleaching, the time lapse
2
3
4 observation was continued every 15 sec. Signal intensities of the nucleus and cytoplasm were
5
6
7 quantified using the MetaMorph software (Molecular Imaging). For RNAi analysis, HeLa cells
8
9
10 were also transfected with siRNA purchased from Invitrogen (for CAND1, PPP2R1A and
11
12
13 PPP2R1B) by Lipfectamin RNAiMAX (Invitrogen). The antibodies against PP2A A subunit and
14
15
16 CAND1 (TIP120A) were purchased from Cell Signaling and Abcam, respectively.
17
18

19 **In vitro transport assay**

20
21
22
23 In vitro transport assay was performed as described in the previous report (Yoshimura et al., 2013).
24

25
26 The detailed procedures of measurement and data analysis are described also in Supplemental
27
28
29 Experimental Procedures.
30
31

32 33 34 35 **Author Contributions**

36
37
38
39 S.H.Y. performed all the experiments and analyses with assistance from technicians. S.H.Y.
40
41
42 designed the study and analyzed the data. S.H.Y., M.K., and K.T. discussed the results and wrote the
43
44
45 paper.
46
47

48 49 50 51 **Acknowledgements**

52
53
54
55 This study was financially supported by a Funding Program for Next Generation World-leading
56
57
58 Researchers (S.H.Y.), a Grant-in-Aid for Scientific Research (B) (S.H.Y.), a Grant-in-Aid for Young
59
60
61 Scientists (A) (S.H.Y.), and a Grant-in-Aid for Scientific Research on Priority Areas (S.H.Y. and
62
63
64
65

1
2
3
4
5
6
7
8
9
10
11
12
13
14
15
16
17
18
19
20
21
22
23
24
25
26
27
28
29
30
31
32
33
34
35
36
37
38
39
40
41
42
43
44
45
46
47
48
49
50
51
52
53
54
55
56
57
58
59
60
61
62
63
64
65

K.T.) from the Japan Society for the Promotion of Science (JSPS), and a Grant-in-Aid for Scientific Research on Innovative Areas (M.K. and K.T.) from the Ministry of Education, Culture, Sports, Science and Technology, Japan. We thank S. Iwasaka, Y. Takashima, M. Minobe and K. Ogawa for technical assistances. The authors declare no competing financial interest. Correspondence and requests for materials should be addressed to S.H.Y. (yoshimura@lif.kyoto-u.ac.jp).

References

- 1
2
3
4
5 Asally, M., and Yoneda, Y. (2005). Beta-catenin can act as a nuclear import receptor for its partner
6 transcription factor, lymphocyte enhancer factor-1 (lef-1). *Exp. Cell Res.* *308*, 357-363.
7
8
9
10 Bayliss, R., Littlewood, T., and Stewart, M. (2000). Structural basis for the interaction between
11 FxFG nucleoporin repeats and importin-beta in nuclear trafficking. *Cell* *102*, 99-108.
12
13
14 Bayliss, R., Littlewood, T., Strawn, L.A., Wentz, S.R., and Stewart, M. (2002). GLFG and FxFG
15 nucleoporins bind to overlapping sites on importin-beta. *J. Biol. Chem.* *277*, 50597-50606.
16
17
18
19 Bednenko, J., Cingolani, G., and Gerace, L. (2003). Importin beta contains a COOH-terminal
20 nucleoporin binding region important for nuclear transport. *J. Cell Biol.* *162*, 391-401.
21
22
23
24 Bednenko, J., Cingolani, G., and Gerace, L. (2003). Nucleocytoplasmic transport: navigating the
25 channel. *Traffic* *4*, 127-135.
26
27
28
29 Bella, J., Hindle, K.L., McEwan, P.A., and Lovell, S.C. (2008). The leucine-rich repeat structure.
30 *Cell Mol. Life Sci.* *65*, 2307-2333.
31
32
33
34 Cho, U.S., and Xu, W. (2007). Crystal structure of a protein phosphatase 2A heterotrimeric
35 holoenzyme. *Nature* *445*, 53-57.
36
37
38
39 Chook, Y.M., and Blobel, G. (1999). Structure of the nuclear transport complex
40 karyopherin-beta2-Ran x GppNHp. *Nature* *399*, 230-237.
41
42
43
44 Chook, Y.M., and Blobel, G. (2001). Karyopherins and nuclear import. *Curr. Opin. Struct. Biol.* *11*,
45 703-715.
46
47
48
49 Cingolani, G., Lashuel, H.A., Gerace, L., and Muller, C.W. (2000). Nuclear import factors importin
50 alpha and importin beta undergo mutually induced conformational changes upon association.
51 *FEBS Lett.* *484*, 291-298.
52
53
54
55 Cingolani, G., Petosa, C., Weis, K., and Muller, C.W. (1999). Structure of importin-beta bound to
56 the IBB domain of importin-alpha. *Nature* *399*, 221-229.
57
58
59
60 Conti, E., Muller, C.W., and Stewart, M. (2006). Karyopherin flexibility in nucleocytoplasmic
61 transport. *Curr. Opin. Struct. Biol.* *16*, 237-244.
62
63
64
65

- 1
2
3
4
5
6
7
8
9
10
11
12
13
14
15
16
17
18
19
20
21
22
23
24
25
26
27
28
29
30
31
32
33
34
35
36
37
38
39
40
41
42
43
44
45
46
47
48
49
50
51
52
53
54
55
56
57
58
59
60
61
62
63
64
65
- Cronshaw, J.M., Krutchinsky, A.N., Zhang, W., Chait, B.T., and Matunis, M.J. (2002). Proteomic analysis of the mammalian nuclear pore complex. *J. Cell Biol.* *158*, 915-927.
- D'Andrea, L.D., and Regan, L. (2003). TPR proteins: the versatile helix. *Trends Biochem. Sci.* *28*, 655-662.
- Denning, D.P., Patel, S.S., Uversky, V., Fink, A.L., and Rexach, M. (2003). Disorder in the nuclear pore complex: the FG repeat regions of nucleoporins are natively unfolded. *Proc. Natl. Acad. Sci. U S A* *100*, 2450-2455.
- Erickson, H.P. (2009). Size and shape of protein molecules at the nanometer level determined by sedimentation, gel filtration, and electron microscopy. *Biol. Proced. Online* *11*, 32-51.
- Fagotto, F., Gluck, U., and Gumbiner, B.M. (1998). Nuclear localization signal-independent and importin/karyopherin-independent nuclear import of beta-catenin. *Curr. Biol.* *8*, 181-190.
- Fischer, E.S., Scrima, A., Bohm, K., Matsumoto, S., Lingaraju, G.M., Faty, M., Yasuda, T., Cavadini, S., Wakasugi, M., Hanaoka, F., et al. (2011). The molecular basis of CRL4DDB2/CSA ubiquitin ligase architecture, targeting, and activation. *Cell* *147*, 1024-1039.
- Forwood, J.K., Lange, A., Zachariae, U., Marfori, M., Preast, C., Grubmuller, H., Stewart, M., Corbett, A.H., and Kobe, B. (2010). Quantitative structural analysis of importin-beta flexibility: paradigm for solenoid protein structures. *Structure* *18*, 1171-1183.
- Frey, S., Richter, R.P., and Gorlich, D. (2006). FG-rich repeats of nuclear pore proteins form a three-dimensional meshwork with hydrogel-like properties. *Science* *314*, 815-817.
- Goldenberg, S.J., Cascio, T.C., Shumway, S.D., Garbutt, K.C., Liu, J., Xiong, Y., and Zheng, N. (2004). Structure of the Cand1-Cull1-Roc1 complex reveals regulatory mechanisms for the assembly of the multisubunit cullin-dependent ubiquitin ligases. *Cell* *119*, 517-528.
- Gorlich, D., and Kutay, U. (1999). Transport between the cell nucleus and the cytoplasm. *Annu. Rev. Cell Dev. Biol.* *15*, 607-660.
- Gorlich, D., Seewald, M.J., and Ribbeck, K. (2003). Characterization of Ran-driven cargo transport and the RanGTPase system by kinetic measurements and computer simulation. *EMBO J.* *22*, 1088-1100.

- 1
2
3
4
5
6
7
8
9
10
11
12
13
14
15
16
17
18
19
20
21
22
23
24
25
26
27
28
29
30
31
32
33
34
35
36
37
38
39
40
41
42
43
44
45
46
47
48
49
50
51
52
53
54
55
56
57
58
59
60
61
62
63
64
65
- Groves, M.R., and Barford, D. (1999). Topological characteristics of helical repeat proteins. *Curr. Opin. Struct. Biol.* *9*, 383-389.
- Isgro, T.A., and Schulten, K. (2005). Binding dynamics of isolated nucleoporin repeat regions to importin-beta. *Structure* *13*, 1869-1879.
- Janssens, V., Longin, S., and Goris, J. (2008). PP2A holoenzyme assembly: in cauda venenum (the sting is in the tail). *Trends Biochem. Sci.* *33*, 113-121.
- Koike, M., Kose, S., Furuta, M., Taniguchi, N., Yokoya, F., Yoneda, Y., and Imamoto, N. (2004). beta-Catenin shows an overlapping sequence requirement but distinct molecular interactions for its bidirectional passage through nuclear pores. *J. Biol. Chem.* *279*, 34038-34047.
- Kotera, I., Sekimoto, T., Miyamoto, Y., Saiwaki, T., Nagoshi, E., Sakagami, H., Kondo, H., and Yoneda, Y. (2005). Importin alpha transports CaMKIV to the nucleus without utilizing importin beta. *EMBO J.* *24*, 942-951.
- Kumeta, M., Yamaguchi, H., Yoshimura, S.H., and Takeyasu, K. (2012). Karyopherin-independent spontaneous transport of amphiphilic proteins through the nuclear pore. *J. Cell Sci.* *125*, 4979-4984.
- Lange, A., Mills, R.E., Lange, C.J., Stewart, M., Devine, S.E., and Corbett, A.H. (2007). Classical nuclear localization signals: definition, function, and interaction with importin alpha. *J. Biol. Chem.* *282*, 5101-5105.
- Lee, S.J., Imamoto, N., Sakai, H., Nakagawa, A., Kose, S., Koike, M., Yamamoto, M., Kumasaka, T., Yoneda, Y., and Tsukihara, T. (2000). The adoption of a twisted structure of importin-beta is essential for the protein-protein interaction required for nuclear transport. *J. Mol. Biol.* *302*, 251-264.
- Liu, S.M., and Stewart, M. (2005). Structural basis for the high-affinity binding of nucleoporin Nup1p to the *Saccharomyces cerevisiae* importin-beta homologue, Kap95p. *J. Mol. Biol.* *349*, 515-525.
- Lubert, E.J., and Sarge, K.D. (2003). Interaction between protein phosphatase 2A and members of the importin superfamily. *Biochem. Biophys. Res. Commun.* *303*, 908-913.
- Marsella, L., Sirocco, F., Trovato, A., Seno, F., and Tosatto, S.C. (2009). REPETITA: detection and discrimination of the periodicity of protein solenoid repeats by discrete Fourier transform.

Bioinformatics 25, i289-295.

- 1
2
3 Mohr, D., Frey, S., Fischer, T., Guttler, T., and Gorlich, D. (2009). Characterisation of the passive
4 permeability barrier of nuclear pore complexes. *EMBO J.* 28, 2541-2553.
5
6
7
8 Naim, B., Zbaida, D., Dagan, S., Kapon, R., and Reich, Z. (2009). Cargo surface hydrophobicity is
9 sufficient to overcome the nuclear pore complex selectivity barrier. *EMBO J.* 28,
10 2697-2705.
11
12
13
14 Neuwald, A.F., and Hirano, T. (2000). HEAT repeats associated with condensins, cohesins, and
15 other complexes involved in chromosome-related functions. *Genome Res.* 10, 1445-1452.
16
17
18
19 O'Reilly, A.J., Dacks, J.B., and Field, M.C. (2011). Evolution of the karyopherin-beta family of
20 nucleocytoplasmic transport factors; ancient origins and continued specialization. *PLoS One*
21 6, e19308.
22
23
24
25 Ori, A., Banterle, N., Iskar, M., Andres-Pons, A., Escher, C., Khanh Bui, H., Sparks, L.,
26 Solis-Mezarino, V., Rinner, O., Bork, P., Lemke, E.M. and Beck, M. (2013). Cell
27 type-specific nuclear pores: a case in point for context-dependent stoichiometry of
28 molecular machines. *Mol. Syst. Biol.* 9, 648.
29
30
31
32
33 Otsuka, S., Iwasaka, S., Yoneda, Y., Takeyasu, K., and Yoshimura, S.H. (2008). Individual binding
34 pockets of importin-beta for FG-nucleoporins have different binding properties and different
35 sensitivities to RanGTP. *Proc. Natl. Acad. Sci. U S A* 105, 16101-16106.
36
37
38
39 Paroni, G., Cernotta, N., Dello Russo, C., Gallinari, P., Pallaoro, M., Foti, C., Talamo, F., Orsatti, L.,
40 Steinkuhler, C., and Brancolini, C. (2008). PP2A regulates HDAC4 nuclear import. *Mol.*
41 *Biol. Cell* 19, 655-667.
42
43
44
45 Ribbeck, K., and Gorlich, D. (2002). The permeability barrier of nuclear pore complexes appears to
46 operate via hydrophobic exclusion. *EMBO J.* 21, 2664-2671.
47
48
49
50
51 Rout, M.P., Aitchison, J.D., Suprapto, A., Hjertaas, K., Zhao, Y., and Chait, B.T. (2000). The yeast
52 nuclear pore complex: composition, architecture, and transport mechanism. *J. Cell Biol.* 148,
53 635-651.
54
55
56
57 Shi, Y. (2009). Serine/threonine phosphatases: mechanism through structure. *Cell* 139, 468-484.
58
59
60
61 Stewart, M. (2007). Molecular mechanism of the nuclear protein import cycle. *Nat. Rev. Mol. Cell*
62
63
64
65

1 Biol. 8, 195-208.

2
3 Sun, C., Yang, W., Tu, L.C., and Musser, S.M. (2008). Single-molecule measurements of importin
4 alpha/cargo complex dissociation at the nuclear pore. *Proc. Natl. Acad. Sci. U S A* *105*,
5 8613-8618.
6
7

8
9 Tamura, K., Fukao, Y., Iwamoto, M., Haraguchi, T., and Hara-Nishimura, I. (2010). Identification
10 and characterization of nuclear pore complex components in *Arabidopsis thaliana*. *Plant Cell*
11 *22*, 4084-4097.
12
13
14

15
16 Tu, L.C., and Musser, S.M. (2011). Single molecule studies of nucleocytoplasmic transport.
17 *Biochim. Biophys. Acta* *1813*, 1607-1618.
18
19

20
21 Wiechens, N., and Fagotto, F. (2001). CRM1- and Ran-independent nuclear export of beta-catenin.
22 *Curr. Biol.* *11*, 18-27.
23
24

25
26 Xu, D., Farmer, A., and Chook, Y.M. (2010). Recognition of nuclear targeting signals by
27 Karyopherin-beta proteins. *Curr. Opin. Struct. Biol.* *20*, 782-790.
28
29

30
31 Yokoya, F., Imamoto, N., Tachibana, T., and Yoneda, Y. (1999). beta-catenin can be transported into
32 the nucleus in a Ran-unassisted manner. *Mol. Biol. Cell* *10*, 1119-1131.
33
34

35
36 Yoshimura, S.H., Otsuka, S., Kumeta, M., Taga, M. and Takeyasu, K. (2013) Intermolecular
37 disulfide bonds among nucleoporins regulate karyopherin-dependent nuclear transport. *J.*
38 *Cell Sci.* *126*, 3141-3150.
39
40
41
42
43
44
45
46
47
48
49
50
51
52
53
54
55
56
57
58
59
60
61
62
63

Figure Legends

Figure 1 - Amphiphilic structure of importin β and its hydrophobic interactions (A) Crystal structure of yeast importin β (Kap95) modified from PDB file 3ND2. The structures of other karyopherin β family proteins and HEAT-rich proteins are also shown in Figure S1. (B) Each HEAT motif contains 2 α -helices: the A-helix (light green) and the B-helix (dark green). (C) Wheel-helix models of the α -helices in HEAT motifs #14–16 of mouse importin β 1. Hydrophobic amino acids are represented by shaded circles. (D) Amino acid composition at the inner and outer surfaces of the HEAT A-helices and B-helices in mouse importin β 1. The distributions of hydrophobic, polar, and charged residues within the helix are summarized.

Figure 2 - HEAT motif-rich proteins pass through the NPC (A) HEAT motif-containing proteins in the human protein database. HEAT motif-rich proteins, which do not belong to karyopherin β family, are listed. The name of the protein, total amino acids, and number of HEAT motifs assigned by the National Center for Biotechnology Information (NCBI) and by our own strategy (Supplemental Experimental Procedures) are shown. The intracellular distribution examined by EGFP-tagged proteins expressed in HeLa cells, $t_{1/2}$ value obtained from FRAP analysis (Figure 3), and the influx rate constant (k_{in}) obtained from the *in vitro* assay shown in (B) are summarized. n.d.: not determined. n.e.: not examined. Asterisk (*) represents the value obtained from HEAT-rich domain fragment and not from the full-length protein. For nuclear accumulation, (-): not detectable, (+): weakly detectable, (++): equivalent to the cytoplasm and (+++): strongly accumulated. (B) *In*

1 *in vitro* import assay of EGFP-fused HEAT-rich proteins. Left panels, images captured at 30 min;
2
3
4 Right panels, fluorescence intensity ratio (nucleus [nuc.] over external [ext.] media) over time, with
5
6
7 or without wheat germ agglutinin (WGA). k_{in} , influx rate constant without WGA; bar = standard
8
9
10 deviation from >5 different measurements. The rate constant obtained here are also summarized in
11
12
13 (A). The import assay results using HA-tagged HEAT proteins are also shown in Figure S2C. (C)
14
15
16 The summary of *in vitro* import assay using HEAT-rich proteins (●) and non-HEAT proteins (◆).
17
18
19 The list of non-HEAT proteins is in Figure S2D. The Stokes radius of the protein was obtained by
20
21
22 gel filtration chromatography using reference proteins (Erickson, 2009). (D) Pull-down assay
23
24
25 between HEAT-rich proteins and nucleoporin. GST tagged Nup62(FG) was incubated with purified
26
27
28 HEAT-rich proteins and analyzed by SDS-PAGE.
29
30
31
32
33
34
35

36 **Figure 3 - Shuttling of HEAT-rich proteins across the nuclear envelope in living cells**

37
38
39 EGFP-fused HEAT-rich proteins were expressed in HeLa cells. The fluorescence signal in the
40
41
42 nucleus was bleached by irradiation with a strong laser (488 nm) at $t = 0$, and then time-lapse
43
44
45 observation continued for 15 min. Fluorescence images at $t = -0.5$, $+0.5$, and 15 min are shown (left
46
47
48 panels). The fluorescence signals from the nucleus (black) and the cytoplasm (gray) were quantified
49
50
51 and plotted against time (right panel). The bars represent the standard deviation of at least three
52
53
54 independent measurements.
55
56
57
58
59
60

61 **Figure 4 - HEAT motif-rich subunit can assist the nuclear transport of CAND1-cullin complex**

1 (A) Crystal structures of a CAND1-cullin1 complex (modified from PDB: 1U6G). CAND1
2
3
4 (HEAT-rich subunit, dark grey) forms a heterotrimeric complex with cullin1 (light grey) and Roc1
5
6
7 (not shown). (B) Pull-down assay between CAND1 and GST-fused cullin (cullin1 [1–497] and
8
9
10 cullin4B [192–638]). Bound (b) and unbound (u) fractions are shown. (C) GST-tagged cullin4B
11
12
13 incubated with digitonin-treated HeLa cells with or without CAND1 was detected by indirect
14
15
16 immunofluorescence with an anti-GST antibody. (D) Control- and CAND1-knockdown HeLa cells
17
18
19 were subjected to immunoblot analysis using anti-CAND1 antibody. (E) FRAP analysis of
20
21
22 EGFP-fused cullin1 (upper panels) or cullin4B (lower panels) in CAND1-knockdown and
23
24
25 control-knockdown cells. Left panels: snap shots prior to bleaching (pre-bleach), after bleaching
26
27
28 (post-bleach, $t = 0$), and 30 min after bleaching ($t = 30$). Right panel: fluorescence intensities in the
29
30
31 nucleus (black) and cytoplasm (grey) of the bleached cell (indicated by an arrow) were plotted
32
33
34
35
36 against time.

37
38
39
40
41
42 **Figure 5 - HEAT motif-rich subunit can assist the nuclear transport of PP2A complex** (A)
43
44
45 Crystal structures of protein phosphatase 2A complex (PDB: 2IAE) (Cho et al., 2007). PP2A is a
46
47
48 heterotrimeric complex with an A-subunit (HEAT-rich, black), B-subunit (regulatory, light grey),
49
50
51 and C-subunit (catalytic, dark grey). (B, C) FRAP analysis of PP2A. The HEAT-rich A-subunit of
52
53
54 human PP2A (PPP2R1A or PPP2R1B) was knocked-down in HeLa cells by RNAi as shown in D.
55
56
57 The EGFP-fused C-subunit (PPP2C α) was expressed, and flux across the nuclear envelope was
58
59
60 analyzed by FRAP as described in Figure 4E. Snapshot images prior to bleaching (pre-bleach), after
61
62
63

1 bleaching (post-bleach, $t = 0$), and 15 min after bleaching ($t = 15$) are shown (B). Bleached cells are
2
3
4 indicated by arrows. Fluorescence intensity in the nucleus was quantified and plotted against time
5
6
7 (C). (D) RNAi of A subunit. Control- and PPP2R1A-knockdown HeLa cells were subjected to
8
9
10 immunoblot analysis using anti-A-subunit antibody. The position of PPP2R1A (~66 kDa) is
11
12
13 indicated by an arrow. The knockdown effect of importin 9, which is known to interact with A
14
15
16 subunit, is shown in Figure S3.
17
18
19
20
21
22

23 **Figure 6 - Conformational changes of HEAT-rich proteins** (A) HEAT-rich proteins firmly
24
25
26 interact with hydrophobic groups. Purified HEAT-rich proteins (importin β , CAND1 and PPP2R1A)
27
28
29 were incubated with octyl-, phenyl-, or butyl-sepharose in the absence (-) or presence (+) of 500
30
31
32 mM NaCl. The bound proteins were analyzed by SDS-PAGE and CBB staining (left panel). The
33
34
35 band intensities from four independent experiments on importin β are representatively quantified
36
37
38 and summarized in the right panel. (B) The fluorescence spectra of purified HEAT-rich proteins in
39
40
41 various solvents indicated were measured at an excitation wavelength of 290 nm. The
42
43
44 solvent-induced shifts of the peak wavelength were plotted against the concentration of alcohol
45
46
47 (mean value from four independent experiments, relative to that in the absence of alcohol). The
48
49
50 direct effect of the solvent on tryptophan fluorescence peak was examined by measuring free
51
52
53 N-acetyl tryptophan in the same solvent, and was subtracted from the results. The results from the
54
55
56 mutants (Trp is replaced by Phe) are summarized in Figure S4D. (C) CD spectra of HEAT-rich
57
58
59 proteins in various organic solvents indicated. The molar ellipticity at 222 nm (the α -helix-specific
60
61
62
63
64
65

1 peak) is plotted against the concentration of organic solvent. In the case of importin β , ~60% of the
2
3
4 molecule is in α -helical conformation, which is in good agreement to the crystal structure (Figure 1).
5
6
7 Raw spectra data are shown in Figure S4F. For simplicity, only mean values from three independent
8
9
10 experiments are plotted.
11

12
13
14
15
16 **Figure 7 - Conformational flexibility is necessary for NPC passage.** Purified HEAT-rich proteins
17
18 were treated with either BS³ (bifunctional crosslinker) or sulfo-NHS (mono-functional group,
19
20 negative control), and then were subjected to the *in vitro* transport assay as described in Figure 2B.
21
22
23 The microscopic images from sulfo-NHS-treated (non-crosslinked) and BS³-treated (crosslinked)
24
25
26 proteins during the time-lapse observation are shown in left panels. The nuclear signal intensity was
27
28
29 plotted against time (right panel). See also Figure S5 for the structural properties of crosslinked
30
31
32
33
34
35
36 proteins.
37

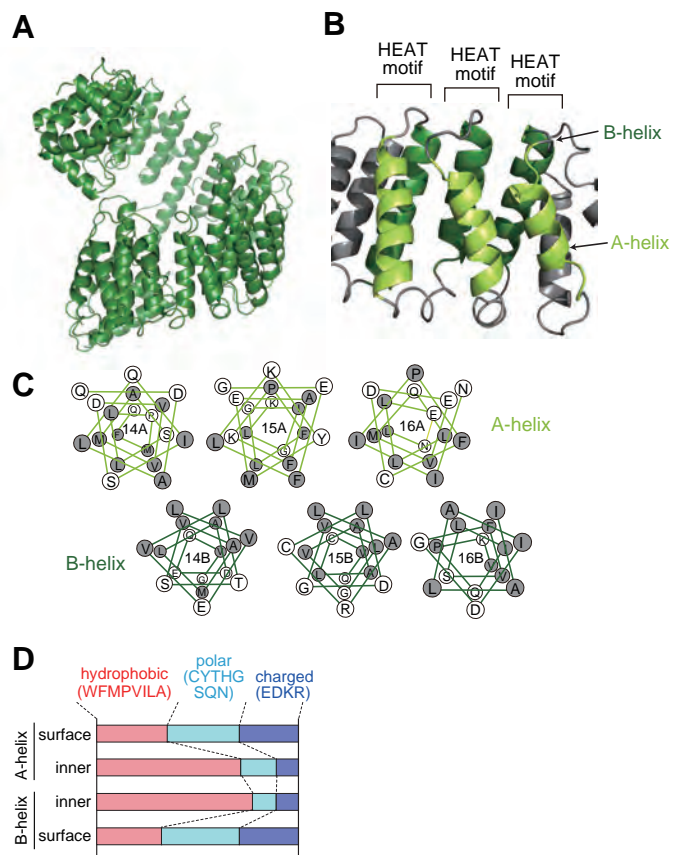
38
39
40
41
42 **Figure 8 - Molecular dynamics simulation of importin β in different solvents** The initial
43
44 structure of importin β (modified from PDB: 1UKL) was mixed with solvent molecules (water or
45
46 50% (v/v) TFE/water), and the molecular dynamics simulation was performed. The RMSd plot
47
48
49 during the simulation time is shown in Figure S6A. One representative result from the 3
50
51
52 independent trajectories is summarized here (A, C, E, and G in water and B, D, F, and H in 50%
53
54
55 TFE). (A, B) Representative structures at 200 ns. (C, D) Changes in the length of each α -helix
56
57
58 relative to the initial state. The bottom panel: color scale (± 10 Å). (E, F) Changes in the distance
59
60
61
62
63
64
65

1 between adjacent HEAT repeats relative to the initial state. The bottom panel: color scale (± 7 Å).
2
3
4 The results from other two trajectories are in Figure S6B. (G, H) Molecular surface representation
5
6
7 with hydrophobic residues in red. (I) Quantification of surface hydrophobicity. The SESA of
8
9
10 hydrophobic residues were quantified by using water molecule as a probe ($r_s = 1.4$ Å) at 200 ns; bar
11
12
13 = standard deviation from 3 trajectories. The detailed evaluation of the surface area is described in
14
15
16 Figure S6C. (J) The hydrophobic SESA was plotted against time. Magenta, importin β in 50% TFE;
17
18
19 Cyan, in water. Importin β was transferred from TFE to water at 100 (light blue) or 200 (dark blue)
20
21
22 ns.

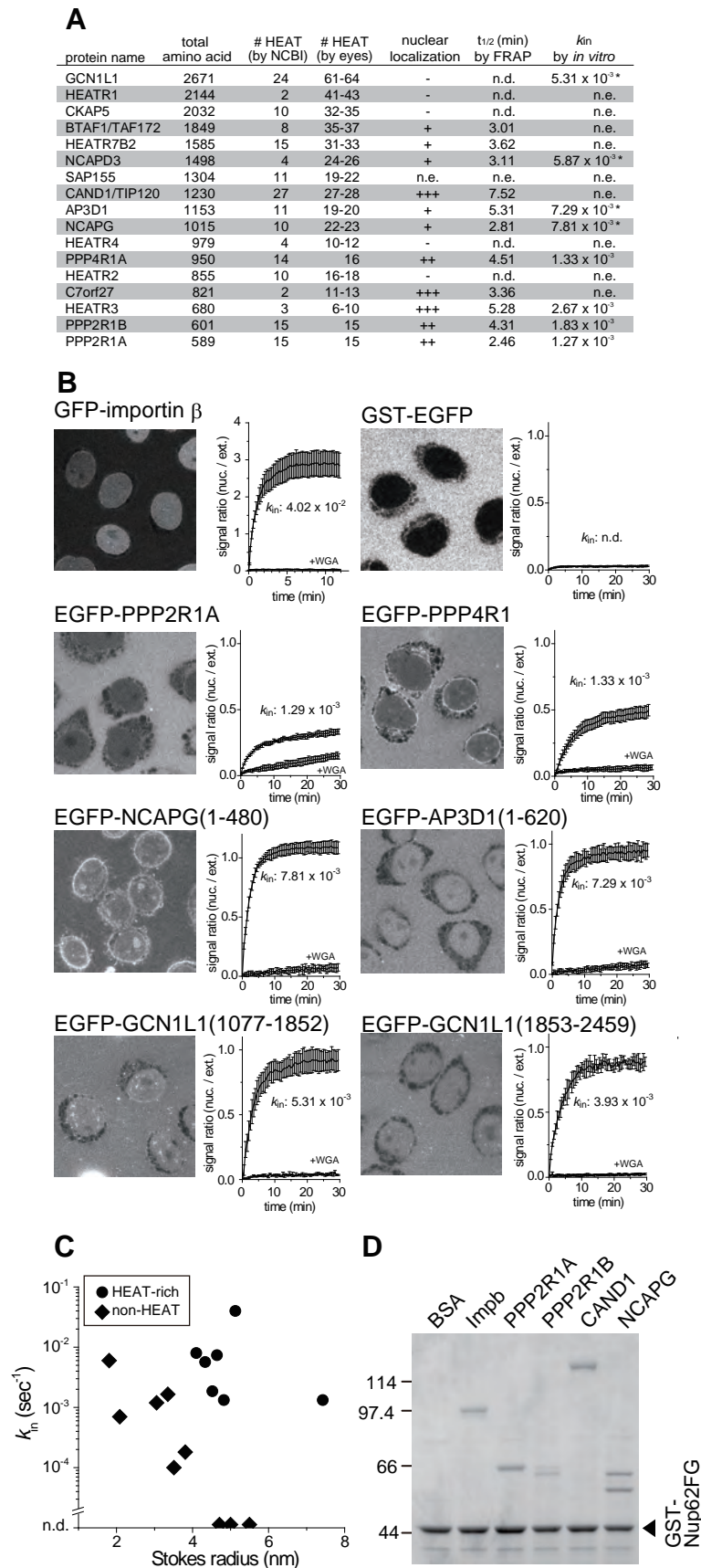
23
24
25
26
27
28
29 **Figure 9 - Structural analysis of cargo-loaded importin β** (A) Pull-down assay between
30
31
32 GST-fused importin β -binding (IBB) domain of importin α and importin β in the presence of
33
34
35 different concentrations of TFE. (B) The effect of TFE on the tryptophan fluorescence peak (blue)
36
37
38 and CD value at 220 nm (red) of IBB-importin β complex was examined as described in Figures 6B
39
40
41 and 6C and summarized. The IBB fragment does not contain any tryptophan residues. (C–H) The
42
43
44 crystal structure of the importin β -IBB complex (PDB: 1QGK) was used as an initial structure, and
45
46
47 was subjected to molecular dynamics simulation in water (C, E and G) and 50% TFE (D, F and H)
48
49
50 as described in Figure 8. Structures at 200 ns (C, D) with IBB in yellow. Distance between adjacent
51
52
53 HEAT motifs (0–200 ns) (E, F). The right panel: color scale (± 7 Å). Molecular surface
54
55
56 representations at 200 ns (G, H). Red, hydrophobic surface; yellow, IBB. The RMSd value and
57
58
59 length of each α -helix during the simulation time are plotted in Figures S6D and S6E, respectively.
60
61
62
63
64
65

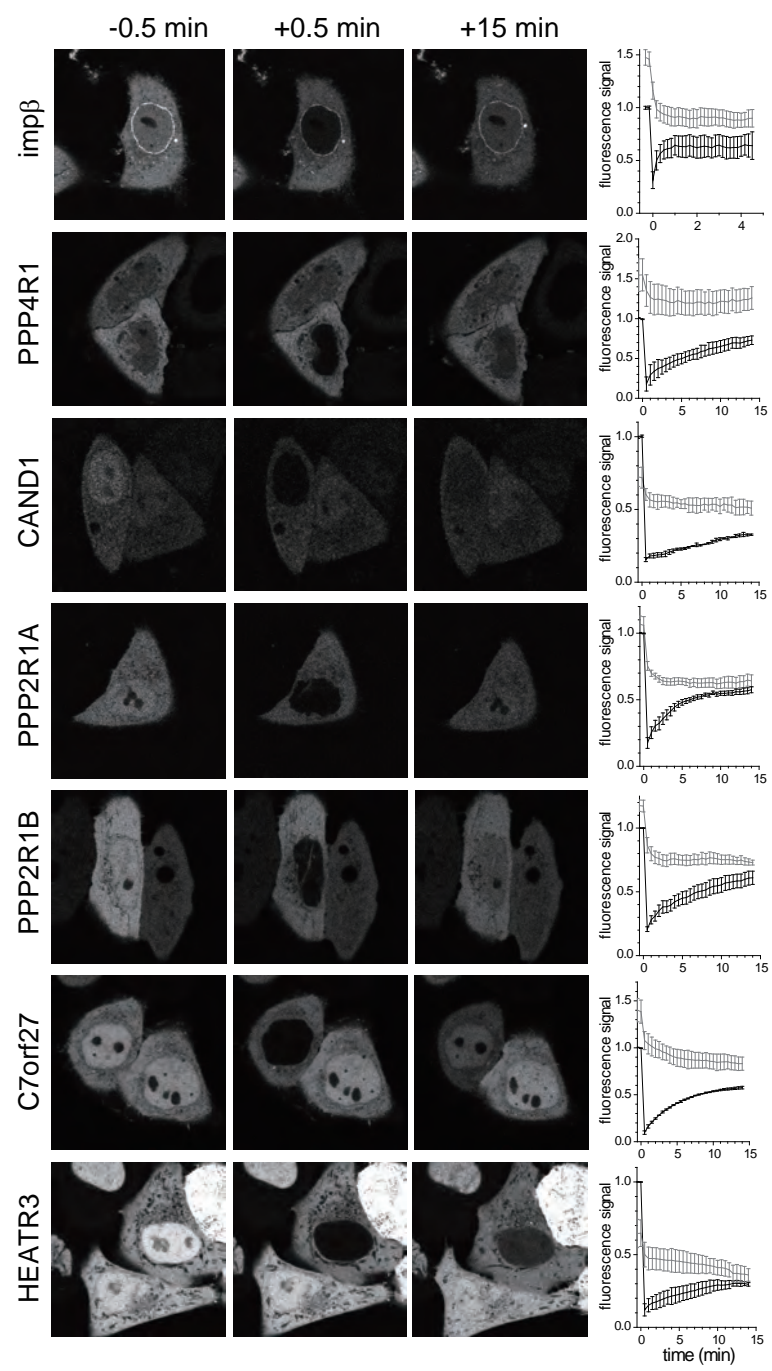
1
2
3
4
5
6
7
8
9
10
11
12
13
14
15
16
17
18
19
20
21
22
23
24
25
26
27
28
29
30
31
32
33
34
35
36
37
38
39
40
41
42
43
44
45
46
47
48
49
50
51
52
53
54
55
56
57
58
59
60
61
62
63
64
65

Figure 10 - Molecular mechanism of protein translocation across the NPC (A) Fundamental mechanism for molecular trafficking through the NPC. Proteins with amphiphilic HEAT motifs pass through the NPC, and in some cases transport bound proteins together. Karyopherins uniquely catch and release cargo proteins in response to nucleoplasm-enriched RanGTP, thus producing a concentration gradient of the cargo across the nuclear envelope. (B) Flexible amphiphilic proteins undergo conformational changes during passage through the NPC. The details are described in the text.

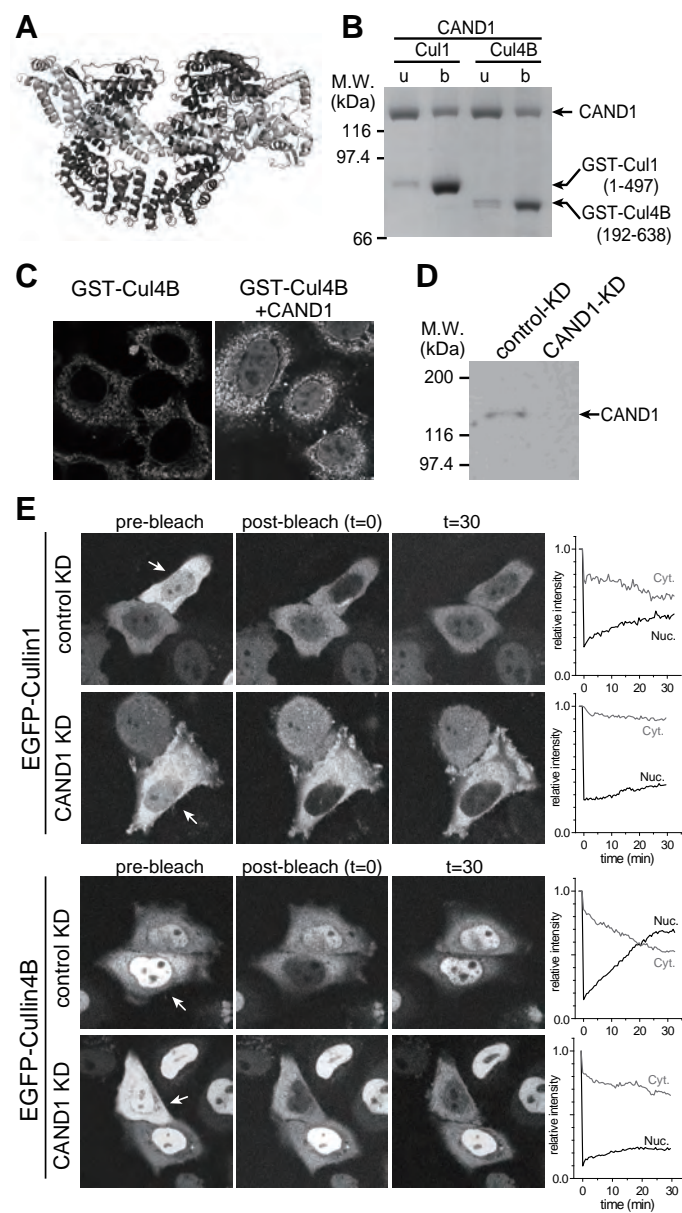


Yoshimura et al. Figure 1

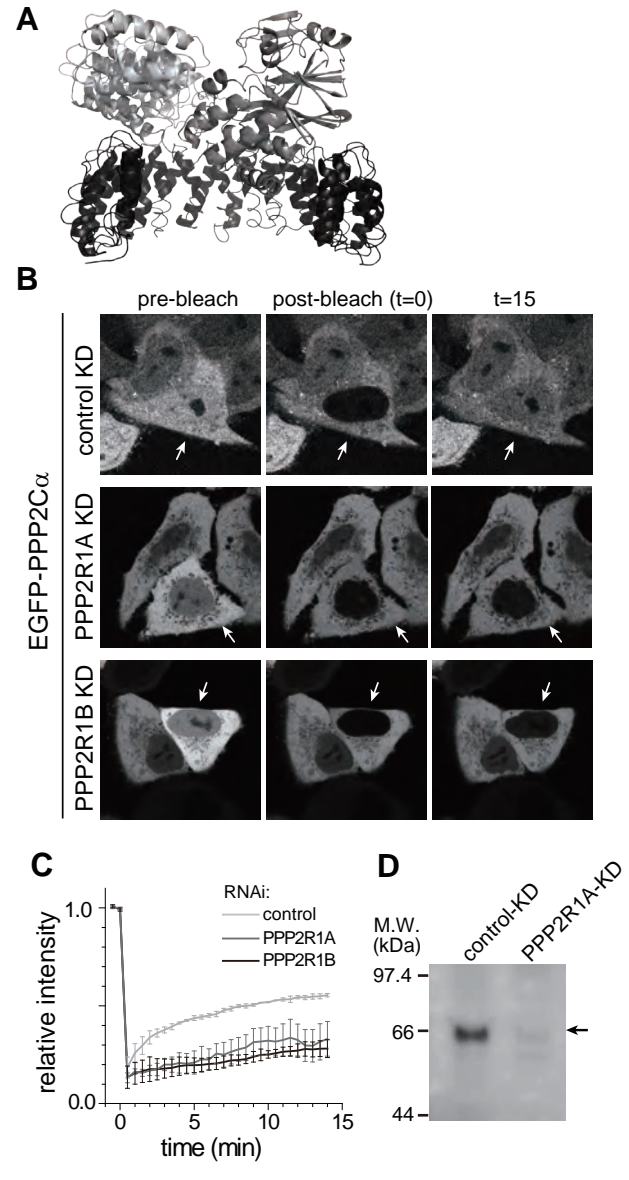




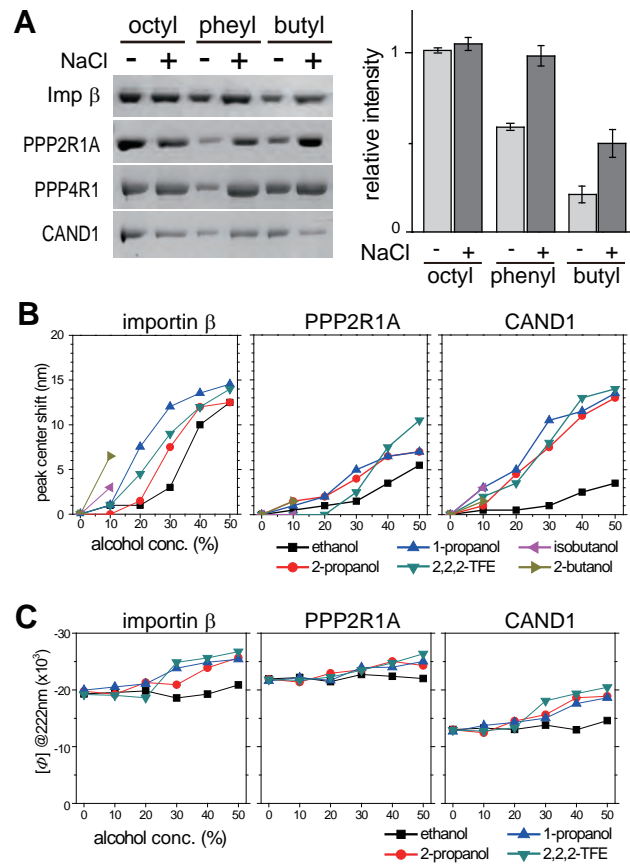
Yoshimura et al. Figure 3



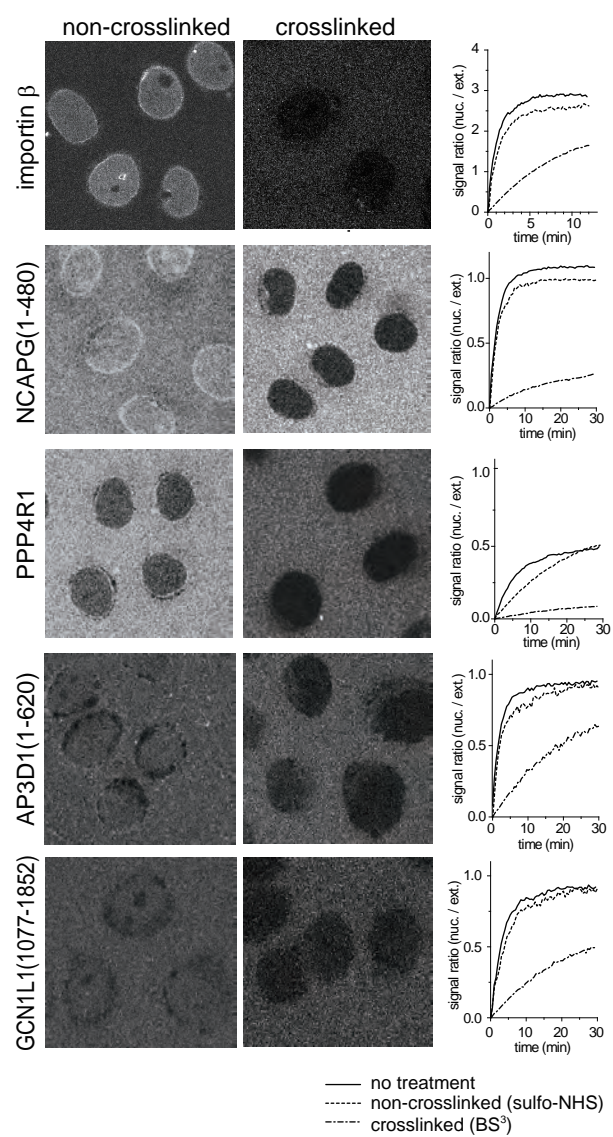
Yoshimura et al. Figure 4



Yoshimura et al. Figure 5

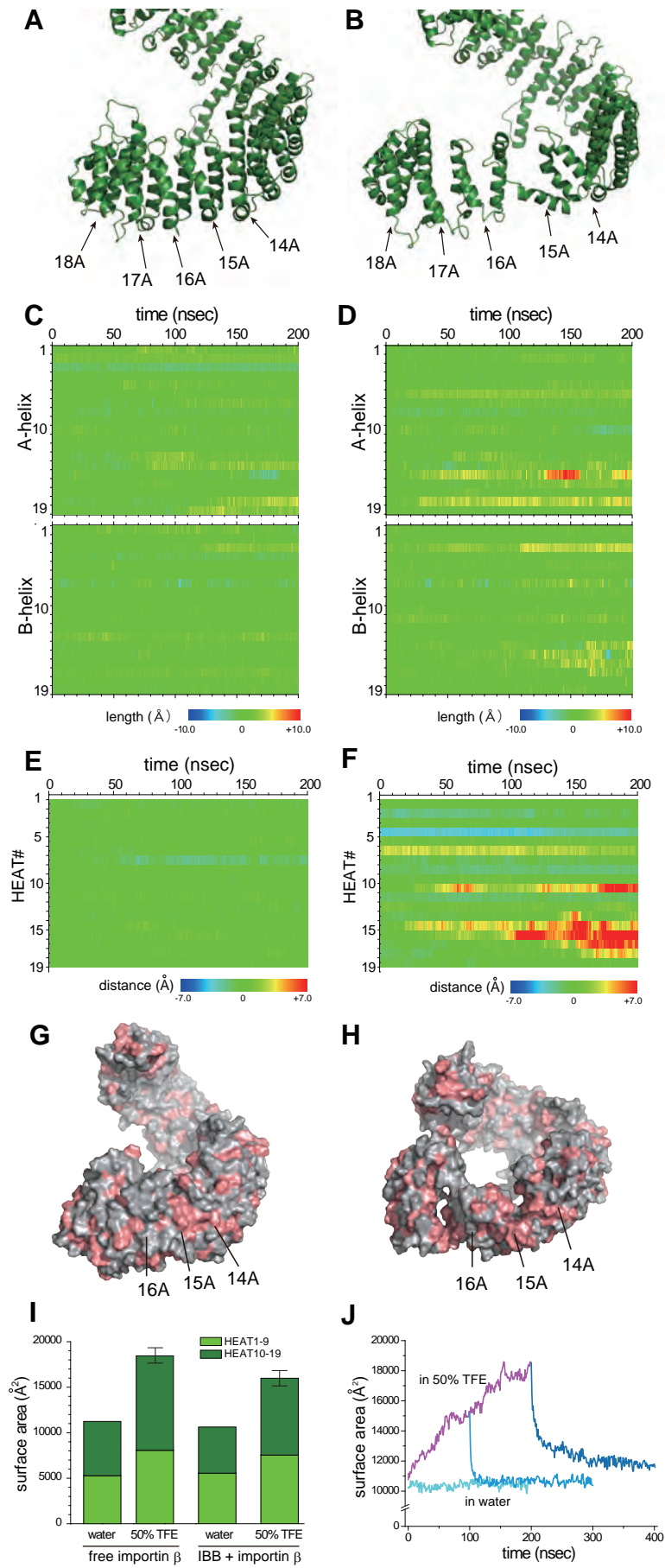


Yoshimura et al. Figure 6

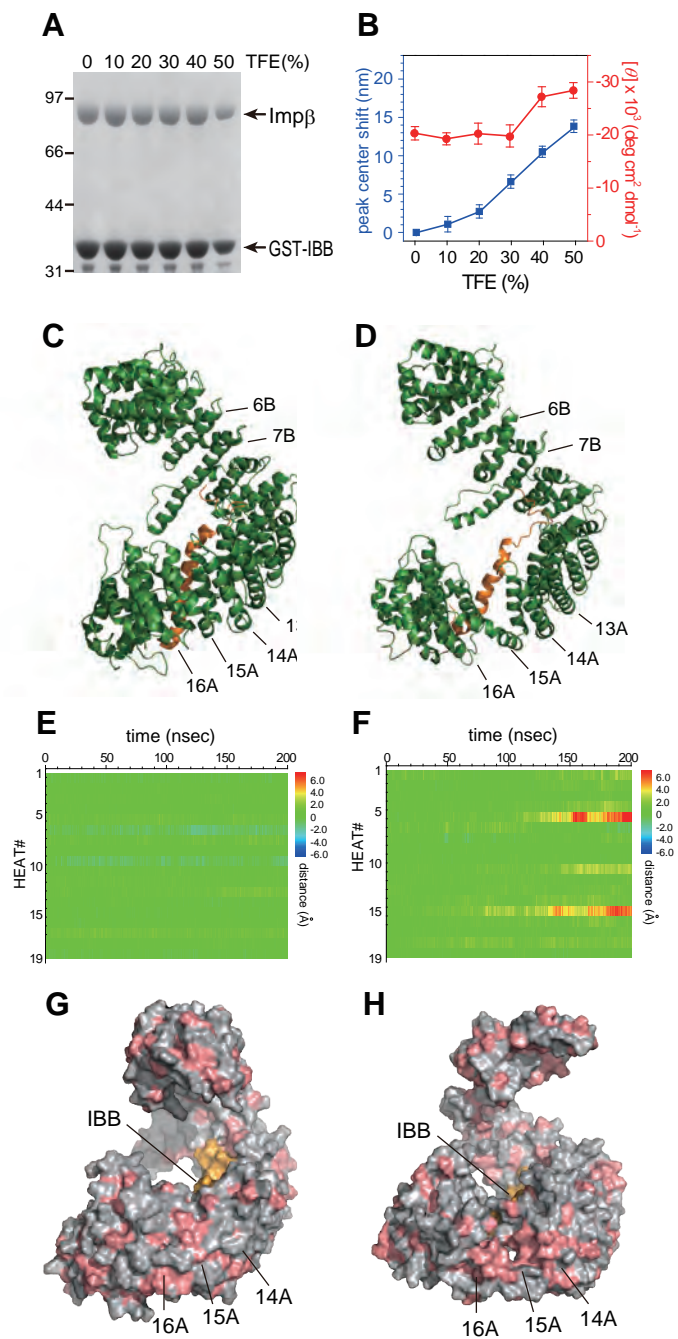


Yoshimura et al. Figure 7

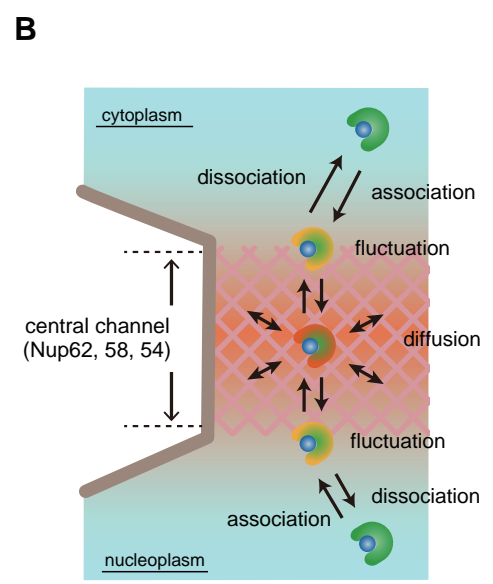
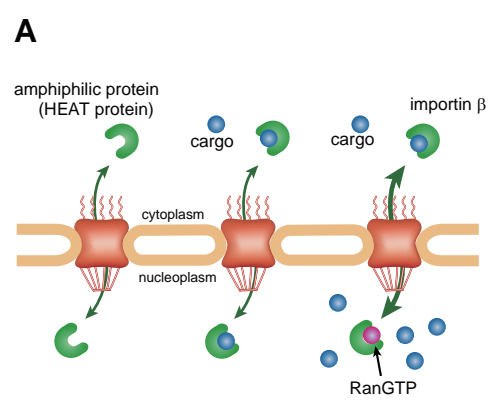
Figure 8



Yoshimura et al. Figure 8



Yoshimura et al. Figure 9



Yoshimura et al Figure 10

1
2
3
4
5
6
7
8
9
10
11
12
13
14
15
16
17
18
19
20
21
22
23
24
25
26
27
28
29
30
31
32
33
34
35
36
37
38
39
40
41
42
43
44
45
46
47
48
49
50
51
52
53
54
55
56
57
58
59
60
61
62
63
64
65

Supplemental Information

**Title: Structural mechanism of nuclear transport mediated by
importin β and flexible amphiphilic proteins**

Authors: Shige H. Yoshimura, Masahiro Kumeta and Kunio Takeyasu

Graduate School of Biostudies, Kyoto University

1 **List of Contents**
2
3

4 **Figure S1, Related to Figure 1; Structure of karyopherin β family proteins and other HEAT**
5
6
7 **motif-containing proteins.**
8
9

10 **Figure S2, Related to Figure 2; HEAT motif-rich proteins pass through the NPC.**
11

12
13 **Figure S3, Related to Figure 5; Involvement of importin 9 in nuclear shuttling of PP2A**
14
15
16 **complex.**
17
18

19
20 **Figure S4, Related to Figure 6; Structural properties of pore-forming FG-nucleoporins**
21
22
23 **(FG-Nups) and alcohol-induced conformational change of HEAT-rich proteins.**
24
25

26 **Figure S5, Related to Figure 7; Characterization of crosslinked importin β .**
27

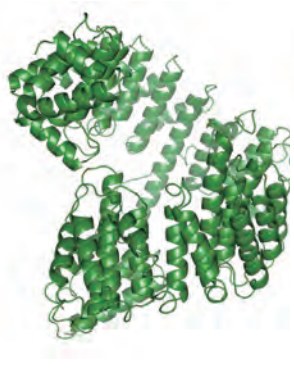
28
29 **Figure S6, Related to Figure 8 and 9; Additional analyses from the MD simulation.**
30

31
32 **Figure S7, Related to Figure 10; importin b contains multiple binding pockets for FG-Nups.**
33
34

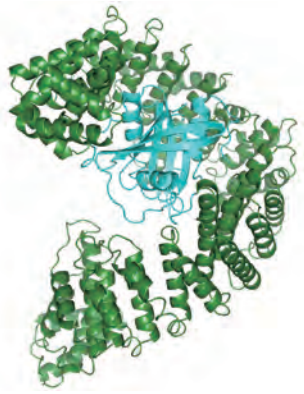
35
36 **Supplemental Experimental Procedures**
37

38
39 **Supplemental references**
40
41
42
43
44
45
46
47
48
49
50
51
52
53
54
55
56
57
58
59
60
61
62
63
64
65

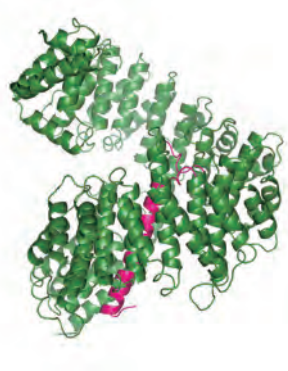
1
2
3
4
5
6
7
8
9
10
11
12
13
14
15
16
17
18
19
20
21
22
23
24
25
26
27
28
29
30
31
32
33
34
35
36
37
38
39
40
41
42
43
44
45
46
47
48
49
50
51
52
53
54
55
56
57
58
59
60
61
62
63
64
65



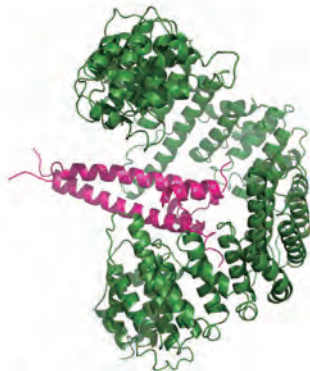
yeast Importin β
PDB: 3ND2



yeast Importin β
+ RanGTP
PDB: 2BKU



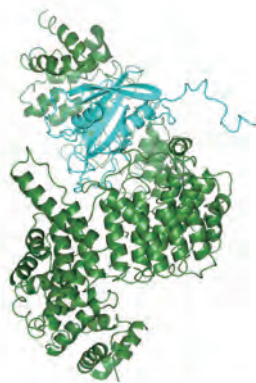
human Importin β
+ importin α IBB
PDB: 1QGK



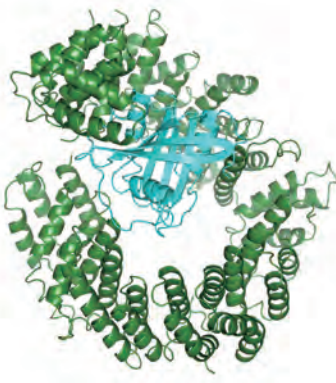
mouse Importin β
+ SREBP2
PDB: 1UKL



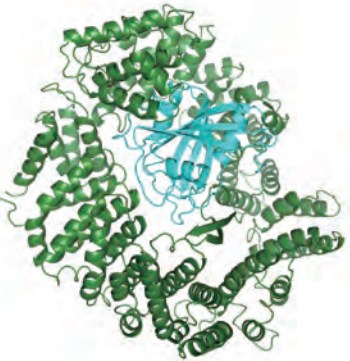
human transportin
PDB: 2QMR



human transportin
+ RanGTP
PDB: 2QMR



human Importin 13
+ RanGTP
PDB: 2X19



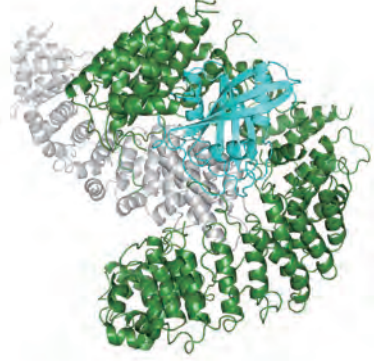
mouse Crm1
+ RanGTP
PDB: 3N1C



yeast Crm1
PDB: 3VYC



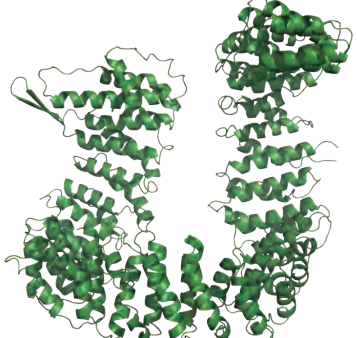
yeast Cse1
PDB: 1Z3H



yeast Cse1
+ RanGTP
PDB: 1WA5



human PPP2R1A
from PDB: 2NYL



human CAND1
from PDB: 1U6G

Figure S1, Related to Figure 1; Structure of karyopherin β family proteins and other HEAT motif-containing proteins. Crystal structures of karyopherin β family proteins (green), and those complexed with RanGTP (cyan) or a cargo (magenta) are shown. In yeast Cse1:RanGTP complex, the cargo (Kap60p) is shown in gray. Non-karyopherin β proteins which contain HEAT repeats (PPP2R1A and CAND1) are also shown.

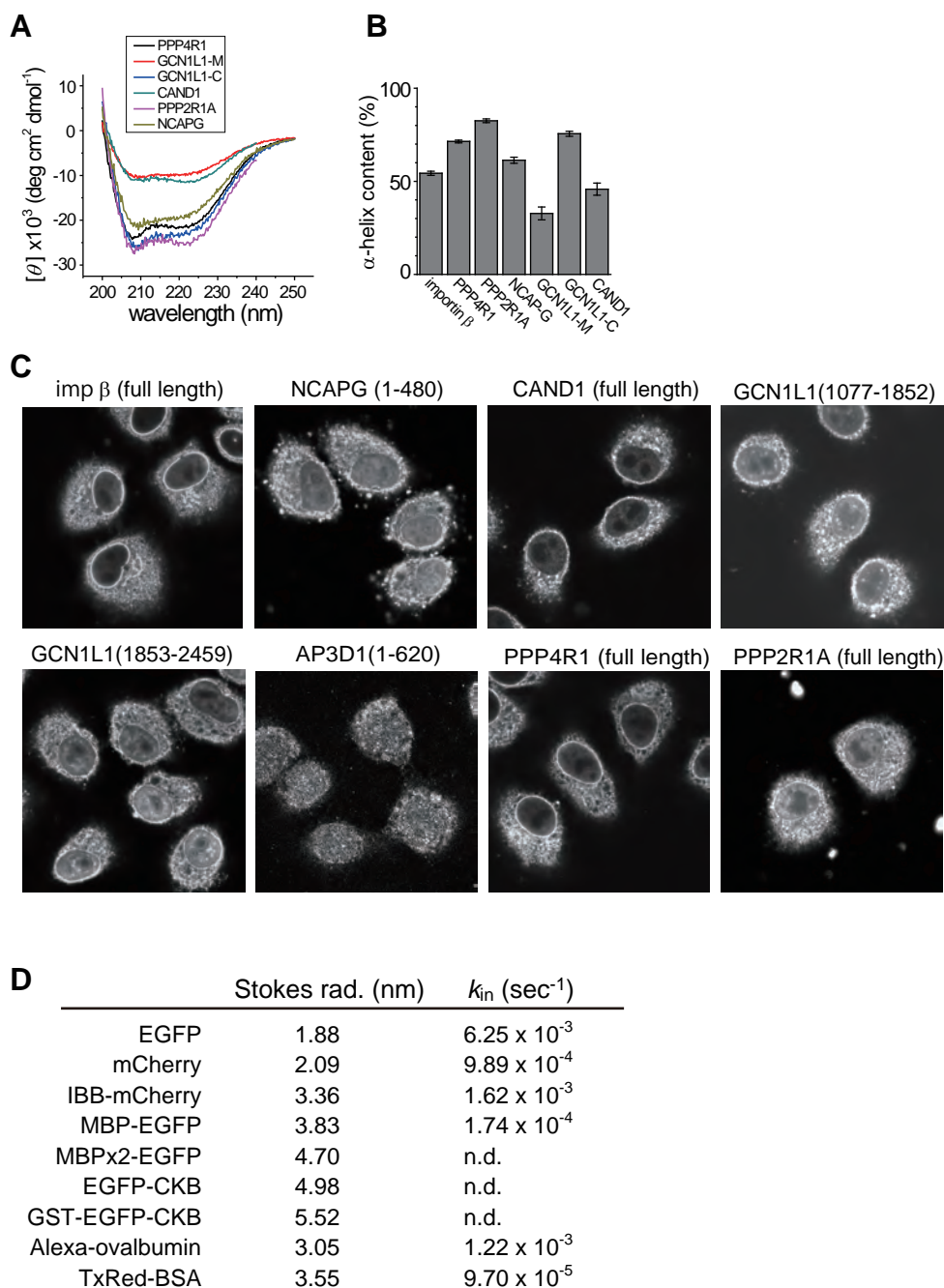


Figure S2, Related to Figure 2; HEAT motif-rich proteins pass through the NPC. (A, B) Circular dichroism analysis of recombinant HEAT-rich proteins. The raw spectra are shown in (A). The α -helix content was calculated based on the molar ellipticity at 222 nm using the following equation: $f_{\alpha} = -([\theta]_{222} + 2340)/30300$, and summarized in (B). (C) GST-HA-tagged HEAT-rich proteins (or protein fragments) described in Figure 2A were expressed as GST-fusion proteins in bacteria, purified by glutathione beads, and separated from the GST moiety by proteolytic cleavage. HeLa cells were treated with digitonin (40 μ g/mL), incubated with the purified proteins at 37 $^{\circ}$ C for 30 min, and immediately fixed with 4% paraformaldehyde for 10 min. The cells were then immunostained with an anti-HA antibody (16B12) and observed by confocal laser scanning microscope. Fluorescence was detected in the nucleoplasm. Fluorescence was also detected in the cytoplasmic region, due to non-specific crosslinking of free proteins in the external solution. (D) The Stokes radius and influx rate constant (k_{in}) of non-HEAT proteins used in Figure 2C are summarized. The Stokes radii were obtained by gel filtration chromatography as described in Erickson et al., 2009.

1
2
3
4
5
6
7
8
9
10
11
12
13
14
15
16
17
18
19
20
21
22
23
24
25
26
27
28
29
30
31
32
33
34
35
36
37
38
39
40
41
42
43
44
45
46
47
48
49
50
51
52
53
54
55
56
57
58
59
60
61
62
63
64
65

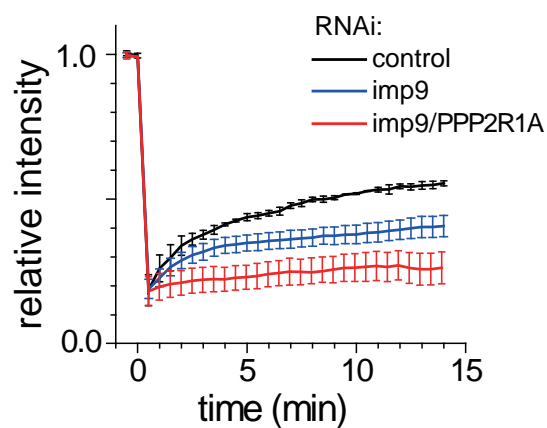


Figure S3, Related to Figure 5; involvement of importin 9 in nuclear shuttling of PP2A complex. FRAP analysis described in Figures 5B and 5C was performed under importin 9-knockdown condition. Knockdown of importin 9 slightly reduced nuclear shuttling of PP2A c subunit. The double knockdown of importin 9 and PP2A a subunit (PPP2R1A) further reduced the rate.

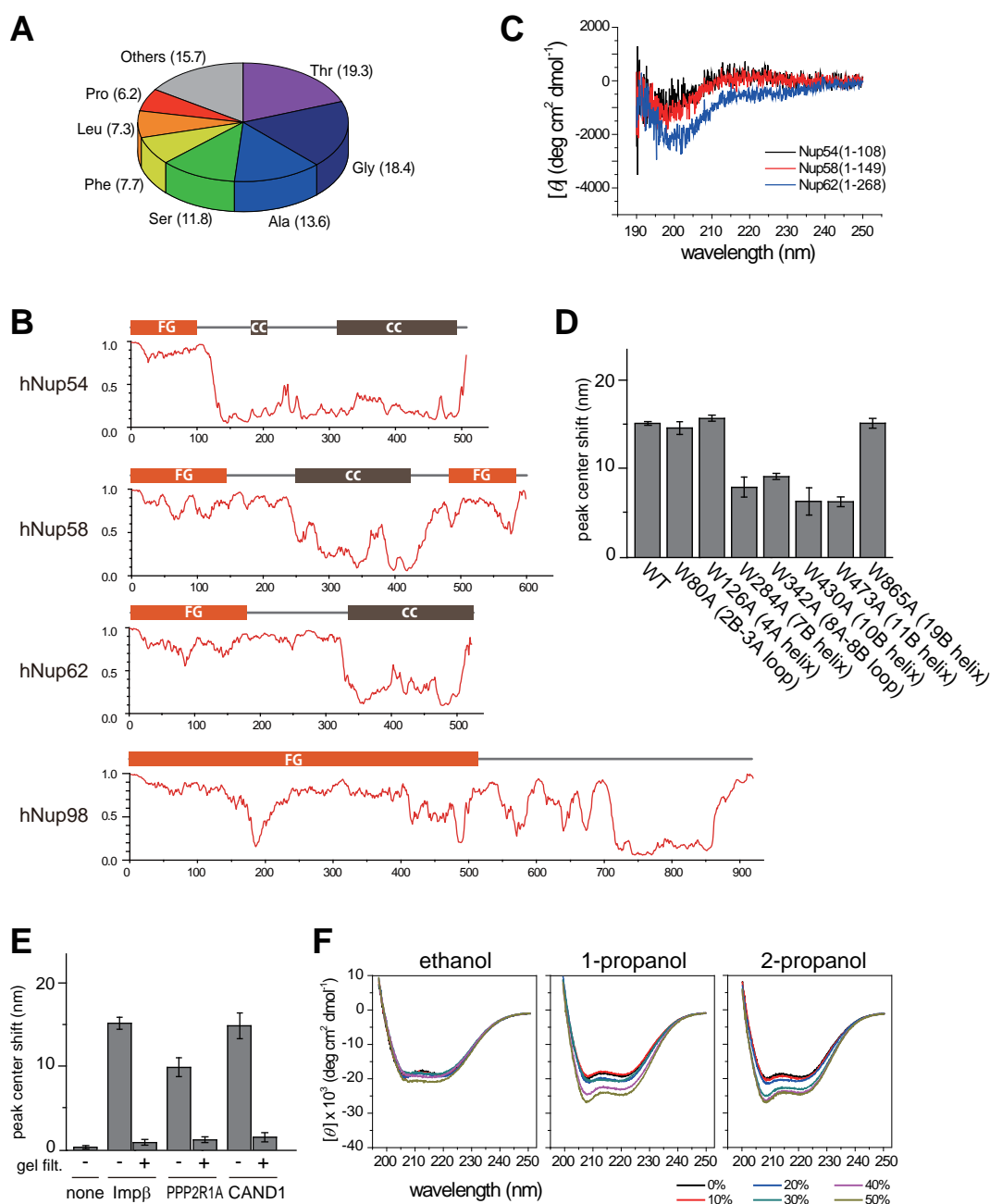


Figure S4, Related to Figure 6; Structural properties of pore-forming FG-nucleoporins (FG-Nups) and alcohol-induced conformational change of HEAT-rich proteins. (A) Amino acid compositions of pore-forming Nups (Nup54, Nup58, Nup62 and Nup98). (B) Structural predictions of pore-forming nucleoporins. The intrinsically disordered regions (IDRs) predicted by the PONDR-fit algorithm are plotted. The coiled-coil regions (cc) and FG-rich regions (FG) are also depicted above the plot. (C) CD spectra of purified IDRs. Human Nup54 (1-108), Nup58 (1-149) and Nup62 (1-268) were expressed in bacterial cells and purified as hexahistidine-tagged proteins, and subjected to CD measurement in 50 mM phosphate buffer (pH 7.4). (D) The analysis of tertiary structures by tryptophan fluorescence. Tryptophan residue in importin β was substituted by phenylalanine, and subjected to fluorescence spectra analysis as described in Figure 6B. The position of the mutated residue in the HEAT repeat is indicated below. (E) Reversible conformational change of HEAT proteins. Purified HEAT-rich proteins were exposed to organic solvent (2-propanol), and subjected to the fluorescence spectrum analysis as described in Figure 6B (-). The exposed proteins were then passed through a gel filtration column to remove organic solvent, and subjected to the same spectrum analysis (+). (F) CD spectra of purified importin β in hydrophobic solvent (ethanol, 1-propanol and 2-propanol). One representative spectrum from three independent experiments is shown.

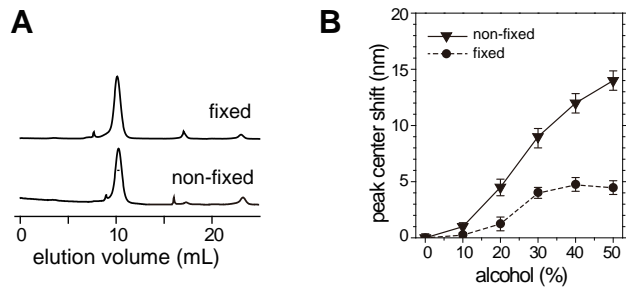


Figure S5, Related to Figure 7; Characterization of fixed importin β . Purified importin β was fixed by a crosslinker (BS³) to restrict conformational changes. Importin β contains 27 lysine residues, 18 pairs of which could be candidates for the crosslinker (spacer length, 11.4 angstroms). The crosslinked protein was subjected to gel filtration chromatography (Superdex 200HR) to examine inter-molecular crosslinking(A), and to the analysis of fluorescence spectrum as described in Figure 6B to examine the structural flexibility (B). The peak center shift was plotted against the concentration of TFE (%).

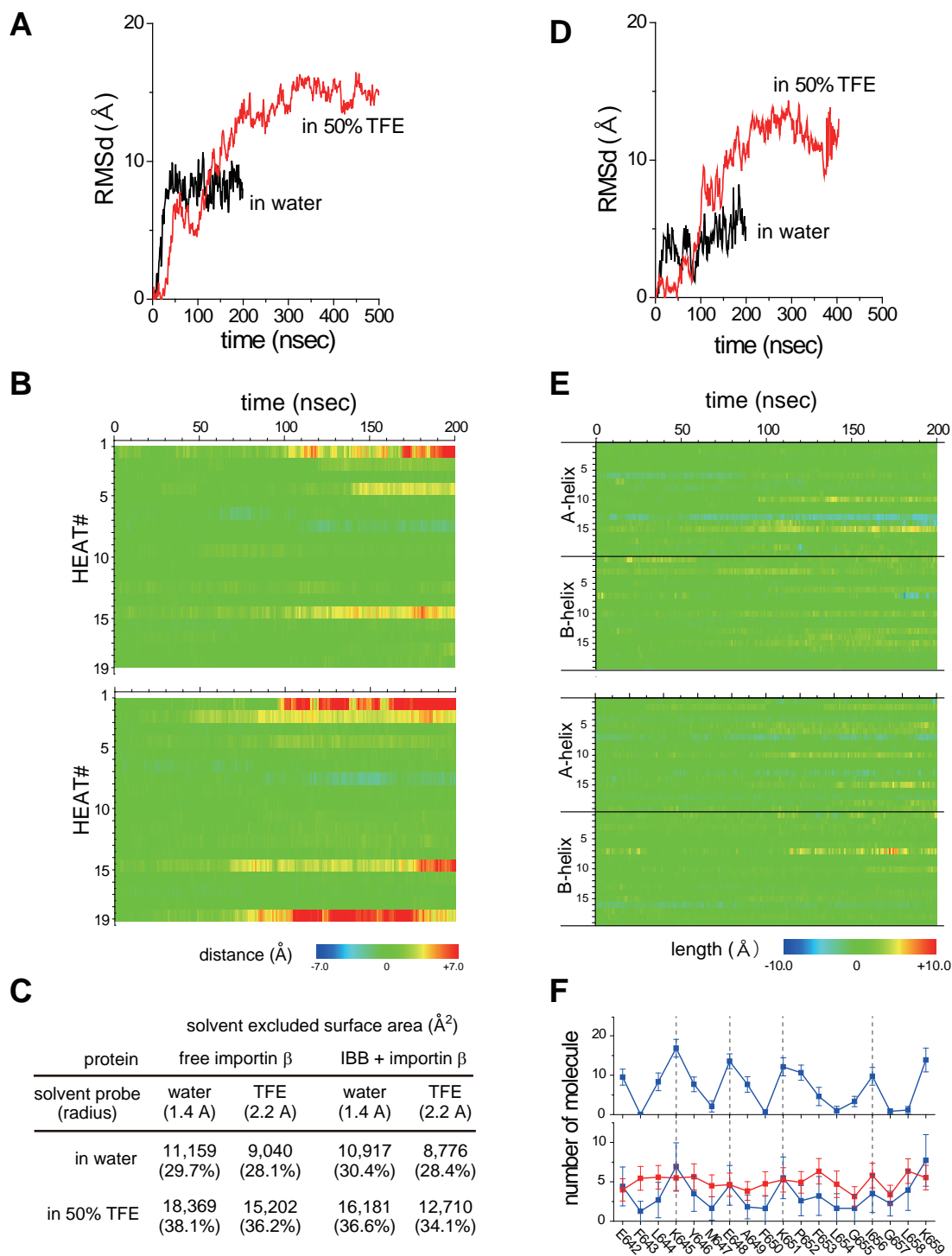


Figure S6, Related to Figures 8 and 9; Additional analyses from the MD simulation. The root mean square deviation (RMSd) during the MD simulation of free importin β (A) and the IBB-importin β complex (D) in water (black) and 50% TFE (red) were plotted against time. (B) HEAT-HEAT distances of importin β simulated in 50% TFE. The simulation and analysis were performed as described in Figure 8. Distances between adjacent HEAT motifs were plotted over simulation time (0-200 ns) for two independent trajectories. Bottom panel: color scale (± 7 Å). (C) Summary of hydrophobic solvent excluded surface area (SESA). The SESA values of hydrophobic residues in free importin β and IBB-importin β in water or 50% TFE at 200 ns were calculated by using two different solvent probes (1.4 Å for water and 2.2 Å for TFE). In both cases, the hydrophobic surface areas were higher in 50% TFE than in water. (E) Helical length of each HEAT motif in IBB-importin β complex in water (top) and 50% TFE (bottom). Changes in the length of each α -helix (A-helix and B-helix, No. 1-19) relative to the initial state were plotted against simulation time. Color scale (± 10 Å). (F) The number of solvent molecules on the protein surface. The number of TFE (red) and water (blue) molecules that are within 5 Å of each amino acid residue in HEAT 15A (E642 - K659) in the simulation in water (upper panels) and in 50% TFE (lower panels) were plotted. The residues that are embedded in a hydrophobic core in water interact with TFE molecules in 50% TFE.

1
2
3
4
5
6
7
8
9
10
11
12
13
14
15
16
17
18
19
20
21
22
23
24
25
26
27
28
29
30
31
32
33
34
35
36
37
38
39
40
41
42
43
44
45
46
47
48
49
50
51
52
53
54
55
56
57
58
59
60
61
62
63
64
65

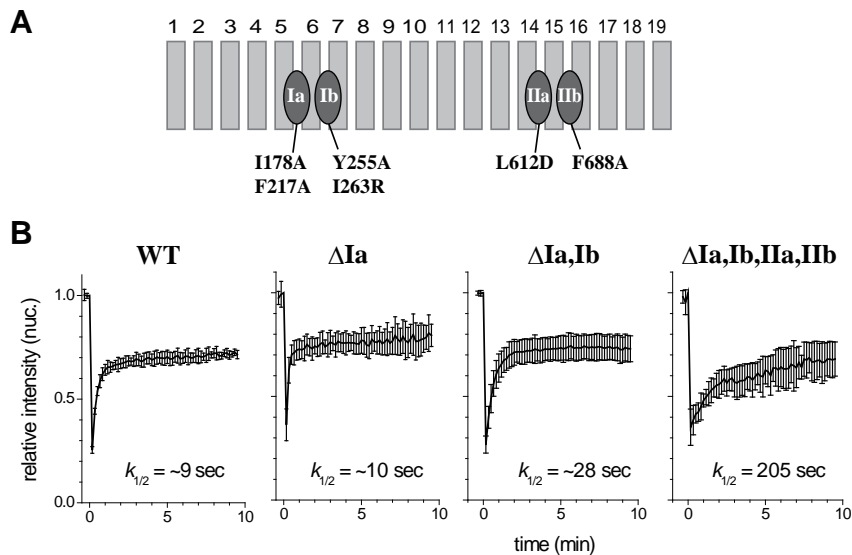


Figure S7, Related to Figure 10; importin β contains multiple binding pockets for FG-Nups. (A) The positions of the binding pockets. The HEAT repeat structure (1-19) of importin β and binding pockets for FG Nups (Ia, Ib, IIa, IIb) are depicted. The amino acid substitutions to abolish the pockets (I178A, F217A, Y256A, I263R, L612D, F688A, described in Bednenko et al., 2003) are also indicated. (B) FRAP analysis of EGFP-Importin β mutants. Importin β which carry mutations in FG-binding pockets were expressed as a fusion protein with EGFP in HeLa cells, and were subjected to FRAP analysis as described in Figure 3.

Supplemental Experimental Procedures

In vitro transport assay

HeLa cells were triple-washed with Transport Buffer (20 mM HEPES-KOH (pH 7.3), 110 mM CH_3COOK , 2 mM $(\text{CH}_3\text{COO})_2\text{Mg}$, 5 mM CH_3COONa , 0.5 mM EGTA, and 1 mM DTT) and incubated with 0.02% digitonin at 0°C for 10 min to remove the cytoplasm and plasma membrane.

The cells were again triple-washed with Transport Buffer, and incubated for 30 min at room temperature to wash away the soluble nucleoplasmic proteins. The nuclei were incubated with purified protein (1–5 μM) and observed every 15 sec for 15–30 min using a confocal laser-scanning microscope (FV1200, Olympus). To check the integrity of the nuclear envelope, 10 $\mu\text{g}/\text{mL}$ Alexa568-labeled IgG was added to the sample. All image analyses were performed using MetaMorph software (Molecular Imaging). Curve-fitting and other kinetic analyses of the obtained data were performed using Origin software (Light Stone).

Calculation of flux rate constant in the in vitro transport assay

To analyze the rate constants (k_{in} and k_{out}) of passage, the movement of proteins from the cytoplasm to the nucleoplasm was approximated as a single-step event, although it occurs in multiple steps in reality: binding from the cytoplasm to the NPC, movement within the NPC, the release from the NPC to the nucleoplasm, and so forth. Therefore, k_{in} and k_{out} represent the rate constants of a net flow across the nuclear envelope, even though a significant part of the imported cargo that binds to the

1 NPC returns to the cytoplasm. The model system consists of 2 compartments, namely the nucleus
2
3
4 (Nuc) and the cytoplasm (Cyt), which are connected by a pore through which macromolecules can
5
6
7 move from one compartment to the other. The rate of macromolecule passage through the pore
8
9
10 depends on the rate constant k and the concentration in the original compartment. Therefore, the
11
12
13 inward and outward rate (v) of importin β movement can be defined as follows:
14
15
16
17
18
19

$$20 \quad v_{in} = k_{in}[\text{Imp}\beta]_{\text{cyto}}$$

$$23 \quad v_{out} = k_{out}[\text{Imp}\beta]_{\text{nuc}}$$

26
27
28
29 The rate of difference in importin β concentration in the nucleus is given by the following equation:
30
31
32
33
34
35

$$36 \quad d[\text{Imp}\beta]_{\text{nuc}}/dt = k_{in}[\text{Imp}\beta]_{\text{cyto}} - k_{out}[\text{Imp}\beta]_{\text{nuc}}$$

$$39 \quad d[\text{Imp}\beta]_{\text{nuc}}/dt + k_{out}[\text{Imp}\beta]_{\text{nuc}} - k_{in}[\text{Imp}\beta]_{\text{cyto}} = 0 \quad (\text{Eq. 1})$$

41
42
43
44
45 In the *in vitro* assay system, the concentration of importin β in the cytoplasm ($[\text{Imp}\beta]_{\text{cyto}}$) is regarded
46
47
48 as constant. Therefore, Equation 1 can be solved as
49
50
51
52
53
54

$$55 \quad [\text{Imp}\beta]_{\text{nuc}} = k_{in}[\text{Imp}\beta]_{\text{cyto}}/k_{out} (1 - \exp(-k_{out} t))$$

56
57
58
59
60
61
62
63
64
65

1
2
3
4 **Finding HEAT motifs in human protein database based on secondary structures**
5
6

7 Amino acid sequences of the HEAT-rich proteins listed in Figure 2A are shown. HEAT motif
8
9
10 positions are highlighted in light (A-helix) and dark (B-helix) green. For PPP2R1A and CAND1,
11
12
13 HEAT motif positions were defined based on their crystal structures. Putative HEAT motifs were
14
15
16 predicted in other proteins using the following procedure: i) avoid naturally disordered regions that
17
18
19 can be predicted by DisProt (underlined regions), ii) predict secondary structures, and iii) check the
20
21
22 amphiphilicity of each α -helix (20-25 a.a. in length) by drawing a helical-wheel presentation. The A-
23
24
25 and B-helices were distinguished based on the existence of proline residues in the A-helix. Red:
26
27
28 acidic residues; blue: basic residues; bold: proline; magenta: proline residues in the A-helix. The
29
30
31 number of proline residues in the A- and B-helices is indicated.
32
33
34
35
36

37 **NCAPG** (1015aa) 22-23 HEAT repeats

38 MGAERRLLSIKFAFLAQQPHONQKLVVALSRTYRTMDDKTVFHEEFIHLYKYVMVVYRREPVERVIEFAAKFVTSFAGSDMEDDEEEDGGLLNLYLFTFLKSHK
39 ANSNVRFRRVCLLINKLLGSMPEVAQDDDFDKINKAMLIIRLKKIPNVRTQAVLALSRLGDPKDECPVVNAYATLIENDSNPEVRRPAVLSCTIAPSAKTLPKIVGR
40 TKDVKAVRKLAYQVLAEKVHMRAMSIAQRVMLLQOGLNDRSDAVKQAMQKHLLQGWLRFSEGNILELLHRDVENSSAVAVSVLNALFSITPLSELVGLCKNNDGRK
41 LIPVETLTPEITALYWCALQEYLSKSGDGEFFLEQILPEPVIYDYLLSYIQSTPVVNEEHRGDFSYIGNLMTKEFIGQQILITIKSLDISEEGGRKLLAVLQETILT
42 LPTIPISLVSFLVERLHITIDNKRTQIVTEIISIRAPIVTVGVNNDPADVRKKEKMAEIKVKLEAKEALENCITLQDFNRASELKEEIKALEDARINLLKETE
43 QLEIKEVHIEKNDATLQKCLILCYELLKQMSISTGLSATMNGIIESLILPGIISHPVYRNLAVALCLGCCGLQNOQFAKIFVLLLVQVQDDVTIKISALKAIFDQ
44 LMTFGILPFKTKKIKLHCEGEENSDEESESKEVEETATAKNVLLSDFLDSEVSELRGAAEGLAKLMFSGLLVSSRILSRLILLWYNFVTEEDVQLRHCLGVFF
45 PVFAYASRTNQCFEEAFLPTLOTLANAPASSPLAEIDITNVALLDTRPSGLNPOAKTSQDYQALTVHONLAMKICNFIILTSFCSPERVYTKALSSLELSSHLA
46 KDLLVLLNEILEQVKDRTCLRALKIKIQLEKGNVEFGQAEAAQDATALTTTTFQNEDEKIKVEYMTPLRGVKATQASKSTQLKTRGGQRKVTVSARTNRRQQTAEAD
47 SEDEVEPEPESEIKVRLPRAKTAALEKSKLNLAQFLNEDLS

48 A-helix with P: 9/22

49 B-helix with P: 10/22

50
51
52 **NCAPD2** (1401 aa), 24-26 HEAT repeats

53 MAPQMYCFHLPLSPPELLKSGGVNQYVQEVLSIKLPPQLRAFQAAFRAGGFLAMLHFDTIYSILHFRSDPGLEKEDTLQFLIKVVSRRHSQELPAIIDDITLGS
54 DRNAHLNALMNCYALIRLESFETMASQTNLVDLGGKGGKARTKAAHGFDWEEERQPLQLLTLQLLDRLHWNHSTIEEFVSLVTGCCYRLLNPTINHQKN
55 RPIREAITHLGVALTRYNHMLSATVKIQMLQHFELAPVLAASVSLWATDGMKSTVGEIVREIGOKCFQELSRDPSGTKGFAAFLELAEVPAITLMSSMCILL
56 HLDGENYMMRNAVLAAMEVVLQVLSQDQLEAAARTRDQFLDTLQAHGHDVNSFVRSRVLQFLTRIVGQKALPLTRFQAVVALAVGRLAQKSVLVCKNAIQLLASF
57 ANNPFSCKLSADLAGPLQKETQKLQEMRAQRRTAAASAVLDPEEEWEAMLPKSTLQQLLQLPQGEIEIPEQIANETTETEDVKGRIVQLLAKASYKKAITLTREAT
58 GHFQESEPFSHIDPEESEETRLNINLGLIFKGAASTQEKNPRESTGNMVTGGTVCKNKNMNSDPEESRGNDELVKQEMLVQYLQDAYSFSRKITEAIGISKMMYEN
59 ITTVVCEVIEFVIVVFPQGVPPQALFGVRRMLPLIWSKEPGRREAVLNAYRQLYLNPKDSARAKAALIQNLSLLVDASVGTIQLCEEILCEFVQDELKPAVTQLL

60
61
62
63
64
65

1 WERATEKVVACQPERGSSVMLLGMMAKPKPEIVGSNLDLTVSIGLDEKFPQDRLAGOVCHAIANISDRKPSLGRKHPFFRLPQEHRLFERLRETVTKGFVHPDPLM
2 IPEKEVAVTLYQLAEGPIVICAGILQGCAQALEKLEEKRTSQEDPKESPAMLPFLLMNLSSLAGDVALQQLVHLEQAVSGELCRRRVLREEQEHTKDPKEKNTS
3 SETTMEELGLVGATADDEAELIRGICEMELLDGKQTLAAFYPLLKVCNPNGLYSNPLSAAASLALGKFCMISATFCDSQLRLLFTMLKSPLEIVRSNLMVATG
4 DLAIRFPNLYDPWPHLYRLRDPAAQVVKTAGLVMTHTLILKDMVKVKGQVSEMAVLLDPEPQIAALAKNFFNELSHKGNAINYLLPDTSRSLPELGVEEEPFHT
5 IMKQLLSYITKDKQTESLVEKLCGRFRSTRTERQQRDLAYCVSQLPLTERGLRKMLDNDFCFDKLSDESIFSAFLSVVGLRNGAKPEKATIDEEQKLRACHTRG
6 LDGIKELEIGQAGSQRAPSAKKPSTGSRYPQLASTASDNDFVTPERPRTRRHNPNTQQRASKKPKVVFSSDESSSEEDLSAEMTEDETPKKTPIILRASARRHS

7 A-helix with P: 9/24

8 B-helix with P: 7/24

10 **SAP155** (1304 aa) 19-22 HEAT repeats

11 MAKIAKTHEDIAEQIREIQGKKAALDEAQQVGLDSTGYDQEIYGGSDSRFAGYVTSIAATELEDDDDDDYSSSTSLLGQKPKGYHAPVALLNDIPQSTEQYDPPFAEHR
12 PPKIADREDEYKHHRRMTIISPERLDPFADGGKTPDPKMNARTYMDVMREQHLTKEEREIRQQLAEKAKAGELKVVNGAAASQPPSKRRRWDQTADQTPGATPKKLS
13 SWDQAETPGHTPSLRWDETPGRAKGETPGATPGSKIWDPTPSHTPAGAATPGRGDTPGHATPGHGGATSSARKNRWDETPKTERDTPGHGSGWAETPRDRGGDSIG
14 ETPTPGASKRKRSDWDETPASQMGGSTPVLTPGKTPIGTPAMNATPTPGHIMSMTPEQLQAWRWEREDERNRPLSDEELDAMFPEGYKVLPPPAGYVPIRTPARKLT
15 ATPTPLGGMTGFHMQTEDRTMKSVDQPSGNLPLFKPDDIQYFDKLLVDVESTLSPPEQKERKIMKLLLIKNGTPPMRKAALRQITDKAREFGAGLFNQILPLLM
16 SFTLEDGERHLLVKVDRILYKDDL RPYVHKILVVIPELLIEDIYARVEGREISNLAAGAATMISTMRPQIDNMDEIVRNTTARAFAVVASALGIPSLLPFL
17 KAVCKSKKSWAQRHTGKIVQOIAILMGCATLPHLRSLVETIEHGLVIEQQKVRTISALATAALAEATPYGIESFDSVLKPLWKGIQGHGKGLAAFLKATGYLPL
18 DAEYANYTREVMLTILIEFQSPDEENKKIVLKVYKCCGTDGVEANYIKTEILPFFKHFWRMALDRRNYRQLVDTTVELANKVGAAEISIRIVDRLKDEAFQY
19 RKNVMEITEKIMGNLGAADIDHKLLEQLIDGILYAFQEQTTEDSVMLNGFGTVVNALGKRKPYLPQICGTVLWRLNKSAAVRRQQAADISRFAVVMKTCGEEKLMG
20 NLGVVLYEYLGEEYPEVLGSLGALKAIVNVIGMVKMTPIKOLLPLRTPILKNRHEKVCENCIDLVGRIADRGAEYVSAREWNRICFELLELLKAHKAIIRATVNT
21 FGYIAKATGPHDVLATLNNLKVQERQNVGTTVAATAIVAEETCSPTVTLALMNEYRVEELNVQNGVLKSLSFLFEYIGEKGDIYAVTPLLLEDALMDRDLVHRQIA
22 SAVVQHMSLGVYFGGEDSLNHLNLYVMNVFETSPLVIAVMGALGLRVAIGPQRMLQYCLQGLFHPARKVRDYYWKIYNSIYIGSDALIAHYPRYINDDKNTYI
23 RYELDYIL

24 A-helix with P: 13/19

25 B-helix with P: 2/19

27 **PPP2R1A** (589 aa) 15 HEAT repeats

28 MAAADGGDLSLYPIAVLIDELRNEDVQLRLNSIKKLSITIALALGVERTRSELLPFLTIITIDEDEVLLALAEQLGHTTLVGGPEYVHCLLPPLFSLATVEITVVRDXA
29 VESLRATSEHSPSLEAHFVPLVKRLAGDQFTSRTSACGLFVSVCPRVSSAVKAEIRQYFRNLCSDDIPMVRRAAASKLGEFAKYLELINVKSEIIPMFSNLASDE
30 DSVRLLAVAEACVNTAQLLPQEDLEALVMPTRLQAAEDKSWRVRMVADEFELQAVGPEITKTDLVPAFQNLKDCAEVRAAAASHKVECELSADORENVIMS
31 QILPCIKELVSDANQHVKSALASVIMGLSPILGKONTIEHLLPLFLAQLKDECEVRLNIISNLDVNEVIGIRQLSQSLLPAIVELADAKIRVRLAIEYMPLLAG
32 DLGVEFFDEKLNLSLCAWLVHYYAIREAATSNLKKLVKFGKWAHATIIPKVLAMSGPNYLHRMTTLFCINVLSEVCGGDITTKHMLPITVLRMAGDPVANVRFNV
33 KSLQKIGPIPDNSTLQSEVVKPILEKLTQDDQDVKYFACALTVLSLA

34 A-helix with P: 13/15

35 B-helix with P: 3/15

37 **PPP2R1B** (601 aa) 15 HEAT repeats

38 MAGASELGTGPGAAGGGDLSLYPIAVLIDELRNEDVQLRLNSIKKLSITIALALGVERTRSELLPFLTIITIDEDEVLLALAEQLGHTTLVGGPEYVHCLLPPLFSLATVEITVVRDXA
39 ATVEETVVRDXAVESLRQISQEHPTVALYAYFVPLVKRLASGDQFTSRTSACGLFVSVCPRASNAVKAEIRQYFRNLCSDDIPMVRRAAASKLGEFAKYLELINVKSEIIPMFSNLASDE
40 IVPLFTSLASDEDSVRLAVAEACVNTAQLLSQDDLETLMVMPTRLQAAEDKSWRVRMVADEFELQAVGPEITKTDLVPAFQNLKDCAEVRAAAASHKVECELSADORENVIMS
41 LPIDRETTIIMNQILPYIKELVSDTNGHVKSALASVIMGLSILGKONTIEHLLPLFLAQLKDECEVRLNIISNLDVNEVIGIRQLSQSLLPAIVELADAKIRVRLAIEYMPLLAG
42 LAITIEYMPLLAGDLGVEFFDEKLNLSLCAWLVHYYAIREAATSNLKKLVKFGTWAQNTIVPKVLMANPNYLHRMTTLFCINALSEVCGGEITTKQMLPITVLRMAGDPVANVRFNV
43 AGDQVANVRFNVAKSLQKIGPIDTALQGEVVKPIVQLKLGQDEDDVKYFACAEATSVALA

44 A-helix with P: 13/15

45 B-helix with P: 2/15

47 **PPP4R1** (950 aa) 16 HEAT repeats

48 MANLSLLQEDLQEDATGFGVDDYSSEDDVIIPPSALDFVSGQDEMLTFLGRLLDKYAASENIFNRMMVARSLLDLEVCDDERDCIAVLERISRLAQQSEPTVRAELME
49 QVPHIALFCCENRPSIPYAFSKFLLPIVVRYLADQNNQVRIKTSQAALLALEQLIERFDVETKVCVPLIELTAPDSNDQKTEAVAIMCKMAPMVGKIDITERLILPR
50 FCIMCCDCRMFHVRKVCANFGDICSVVGGQATDEMILLPRFFQLCSQNVVWGRKACAECFMAVSCATCGEINRTKLSALFINLISDPSRWWQAFQSLGPFISTFAN
51 PSSSGQYFKEESKSSSEEMSVENKNRTRDQEAPEDEVQVRPEDTPSDLSVSNSSVILENTMEDHAAEASGKPLGEISVPLDSSLCTLSSESHQEAASNENDKKPGNYKS
52 MLRPEVGTTSQDSALLDQELYNFHFWRTPLEIDLDIELQNSGGKPSPEGPEEESGVPVSSPNIIMATRKLEEMTENLEPHIDDPDVKAQVEVLSAALRASLSD
53 AHETISTIEKRSDLQDELINELPNCKINQEDSVPLISDAVENMDSTLHYIHSDSDLSNNSFSFDEERRTKVDVYEQALLDQYLSMTIPPSRAQTVDEIAKHCAYS
54 PGVALTLGQNVHCLRETYETLASIQMOWKVRRLAFSIFELAVILGDLQTAADVIFNGFLKQLDQVRIQVLRKHFDLKLHDKRREYLYQLQCFVTDNSRNV

55 A-helix with P: 13/15

56 B-helix with P: 2/15

RFRLEAEQLILL ELYSPROVYDYLFPIALNLCAIKVSSVRVWISYKLVSEEMVKLHAATPTTFGVDLINLVENFGFCPKWSSGRGAFVFCQTVIEDDCLFMDQFAV
HLMFHLTLANDRVPVRRVLLAKTLRQTLLEKDYFLASASCHQLAVEQTIMALQMDRSDSKYFASTHPASTKISEDAMSTASSTY

A-helix with P: 11/16
B-helix with P: 7/16

CAND1 (Cullin-associated NEDD-dissociating enzyme) (1230 aa) 27-28 HEAT repeats

MASASYHISNLLKMTSSDKDFRMAINDLMTLELQDSIKLDDSEKRVVVMILKLLKEDKGEVONLAVKCLGPLVSKVKEYQVETIVDTLCTNMLSDEQLRDISS
SLKTVICELPPASSGSAANVCKKITGRLLTSAIAKQEDYSVOL EALD IADNLSRGGLLVNFHPSILTCLLPQLTSPRLAVRKRITIALGHVMSCGNIVFVLLIE
NLLSELKNDMSMSTRFYIQCIAAISRQAGNRIGEYLEKIIPLVVKFCNVDDDELECYIQAFESFRRCPKEVYPHVSTIINICLKYLYTDPNYNYDDEDEDENAM
ADGGDDDDQGSDDDEYSDDDMSKVRRAAAKCLDAVVSIRHEMLPEFYKTVSPALISRFKEREEVVKADVFHAYLSLLKGRPVQSWLCCPDAMEQGETPLTMLQSQV
FNIVKALHKQMKKSVKTRQCCFNMLTELNVNLPGALTOHIPVLVPGIIFSLNDKSSSNLKIDALSCLYVILCNHSPQVFFHVPVQALVPPVVACVGDPEYKITS
LVTQQLVKVIRPLDQPSFDATFYIKDLFTCTIKRLLKAADID:EVKERATSCMGQITCNLGDNLGSDLPNTLQIFLRLKNETRRLTTVKALTLIGSPLKIDLRFVL
GEGVPILASFLRKNIPALKGLTALSADLTKNYSDSLTAAMI DAVLDELPLISESDMHSQMAISFLTTLAKVYPSLSKISGSILNELIGLVRPPLLGGALSAM
DFFQALVVTGTNNLGYMDLLRMLTGPVYSQSTALTHKSYSSIAKCVAAITRACPKGPAVVGQFIQDVKNRS:DSIRLLALLSLGVEGHRDLSGQLELKSIVLEA
FSSPEEKSAASYALGSISVGNLPEYLPFVLQEITSQPKRQYLLHSLKEIISASVVGKPYVENIWAALLKHCAEESTRNVVAECLGKTLIDPETLLPRKKG
YLISGSSYARSSVAVKFTISDHPQPIQFLKNCIGDFLKTLEDDLVNRRVALVTFNSAAHFKPSLRDLDLDTVLPHLYNETKVRKELIREVEMGPFKHTVDDGLD
RKAAR-ECMYTLLD:CLDRLEDFEFLNVEDGLKDYD:KMLTFLMLVRLSTLCP:SAVLRQLRRLVEPLRATCTTKVKAN:SVKQEFKQDEKRSANRAVAAL:TIPE
AEKSPLMSEFQSQISSNPELAAIFESIQKDSSTNLESMDS

A-helix with P: 20/27
B-helix with P: 1/27

AP3D1 (AP3 complex subunit delta) (1153 aa) 19-20 HEAT repeats

MALKMVKGSI DRMF DKNLQDLVRGIRNHKEDEAKYISQCIDEIKQELKQDNI AVKANAVCKLTYLQMLGYDISWAAFNI:EVMSASKFTFKRIGYLAASQSFREGTDY
LMLTTNQIRDLSSPSQYOTGVALTGLSCFVTPDLARDLANDIMTLMSTKPYIRKKAVLIMYKVFLLKYPESLRPAFPRLKEKLEDDPDPVQSAAVNVI:CELARLNPK
NYLSLAFLFFKMTSSTNNVFLKIKLFGALTPLEPLGKKLEPLTNLIMSTAMSLLYECVNTVIAVLSLSSGMPNHSASIQLCVQKLRILIEDSONLKYLGL
LAMSILKTHPKSVQSHKOLILQCLDDKDESIRLRALDLYGMVSKNLMETVKKLMTHVDKAEGTTYRDELTKIIDICSSNYQYITNFEWYISILVELTRLEGFR
NGH:IAAGMLDVAIRKAIKFAVSOALSALLSASTQ:NGTCEVLYAAAWTCGEFS:EHLEPEHHTL:AMLRRVTTLP:GH:QAVYVQNVVKLYASTLQOKEQA
GEAFGAQAVTQLMVDRLPQFVQSADLEVOEXASCTLQLYKRTIKLQAKDVVAEEVSALFAGELN:VAPKAQKKVPVPEGLDLDAWINEPLSDSESEDERPRAVFHEE
EQRRPKHRPSEADEEELARRREARKQEQANNPFYIKSSPSPKRYQDTPGVEHIPVYQIDLSVPLKVPGLPMSDQYVKLEEEERRHRQKLEKDKRRKKRKEKEKKGKRR
HSSLPTESDEDIAPAQQVDIVTEEMPEALPSDEDDKDPNDPYRALDIDLKPLADSEKLP:IKQHRNTE:TSKSPKDVPMVEKSKPKPKKKEKHKHEKERDKKPKKKEK
EKKKSPKPKKKKHKRKEKEERTKGGKSKKQPPGSEEAAGEPVQNGAPEEEQLPPESSYLLA:ENSYVNTOD:RGSLEDSQVTVAVILENRSSSILKGMELSVLDSL
VARMARPGSSVHDGVVVFQLPFGVSN:EAQVFTIQSIVMAOKLGLTSLFA:KNDEGATHEKLD:FRLHFSCSSYLITTY:GY:DFAKLESGDLSMSSKVDGIRMS
FQNLLAKICFHHFSVVER:DSCASMYRS:QGHVCLLVKKG:ENSVSV:DGKGS:STLLSNL:EEMKATLAK

A-helix with P: 9/20
B-helix with P: 3/20

HEATR2 (855 aa) 16-18 HEAT repeats

MAALGVAEVAAPHPAEGAETA:EAVELSRALSRLLPGLEADSKPGRRRAL:EARLRALEEPGPAADPTAFQGPWARLLLPRLLRCLSDPAEGCRALAVHLLDLGLRRAA
RPRDALPRLPALAARLAGVPARRPPEACEELRLALVQLLGLAVDLGGAALAPHLDDALRALRCSLLDPFAAVRESCSCAAAALAA:PDHFHMQS:SLIGPLMGTI
S:QH:K:RVAAIEATGAV:IFGNGK:SVDDVLSHFQRLFDV:PVRR:AVASVVGWLLCL:RDRYSFFHKLIPLLSSLN:EVPE:RQLAASL:EDVGLQWQKENEEDL
KDKLDFAPPTPPHYPPHERRPVLGCRFLVFNLSKILPALCHDITDWWVGR:KSAQLLPVLL:HAEDH:ATOHL:EVVLR:TLFQACT:DEE:AAVQSG:TRSAELVGFVS
PEVFLKILSTLKKTPSASG:LVLASAMRGP:PREALOPHLAAIATELAGAHI:QASENDLY:ERLL:CVQALVSV:HE:GVASLQLLDVLLTIVALAGATGLR:K:KQ
ET:DSLAM:EGVSSQ:DLRYKH:IGP:LLERV:TASHLD:WTA:SP:ELQFSV:VAGS:PAL:GEALPHV:V:TLRACLQ:PSQ:DPQMR:KLF:SLSTVLL:RAT:DTINS:QGG:PS
YLET:VT:K:QILAP:NLQ:IPACRTAAAT:RTAAV:SQLWALTSS:EVLSA:EQIR:QVQ:ETLM:QVLT:LEED:SKITRL:ISCR:INTFL:KTS:GGM:DP:EKLIRIY:PELLKRL:DVVS
NDVR:MAAASLTVTWLCQV:KGANAKSY:QSSVQYLYRELLVHL:DP:PER:ATQD:ILEVLEK:EGSGL:PD:LLVRETE:AVI:HKHR:SATYCEQLLQVQVAPATQ

A-helix with P: 10/16
B-helix with P: 2/16

CKAP5 (2032 aa) 32-35 HEAT repeats

MGDDSEWLKLPVQKCEHLWKARLSGYEEALKIFCKIKDEKSP:EWKFLGLIKKFVTD:SNAAVQLKLEAALVYVENAHVAGKTTGEVVGVSVKVFNQPKAKKEL
G:IEGLMYE:EKSEAVQ:PELLGLDNKPKIIVAC:ETLRKALS:EFGSKI:ILLKPIIKVLPKLFESRE:KAVRDEAKLIAVETIRWIRDALPPLONINSVOLKLEEE
EWWKLP:TSAPRPRFLRSQ:LEAKLEQQQSAGGDAEGGGDDGDEVPQIDAYELLEAVEILSKLPKDFYDKIEAKKWQER:KAL:ESVEVLK:KPKLEAGDYADLVKAL
K:YVGD:TNM:VALAAK:CLTGLAVGL:RKK:FGQYAGHV:PTILFKFKKPPVQVALQEAIDAITLTTLQNI:SEV:LVAVM:DNK:PTI:KQQ:SLFLIARSRHCTASTL
PKSLLK:FCAALLKHINDSAP:EV:DAAF:EA:LG:AL:KVVGEKAVN:PFLAVDKL:KDK:KECSEKVEL:HGK:KAGLAADKKEFKPLPGR:TAASGAAGDKD:KDISAPKP
GPLK:KAPAAKAGGPPKKGKPAAPGGAGNTGTKNKKGLE:KEIVEPELSIEVCEE:KASAVL:PP:TC:IQLLDSSNWKER:LACHEEFQKAVELM:DRTE:MP:CGALVRMLANKP

1
2
3
4
5
6
7
8
9
10
11
12
13
14
15
16
17
18
19
20
21
22
23
24
25
26
27
28
29
30
31
32
33
34
35
36
37
38
39
40
41
42
43
44
45
46
47
48
49
50
51
52
53
54
55
56
57
58
59
60
61
62
63
64
65

1 GIKETNFQVMQMKLHIVALIAQGNFSKTSQAQVLDGLVQKIGDKOGNNAKEAMTAIAACMLPWTAFQVVSMAFSQKNPKQSEETLNWLSNAIKKGFSGLNVKAF
2 ISNVKTLAALATNPAVRTAAITLQVMYLYVGLSLRMFFDEKPAALLSQIDAEFEKMQGQSPAPTRGISKHSTSGTDEGEDGDEPDDGSDVVDLLPRTETISDKITSE
3 LVSIGDKNWKIRKEGLDEVAGIINDAKFTQPNIGLPTALKGRNDSNKILVQOITLNILOQLAVANGPNIKQHVKNLGIPTITVGLGSKNNVRAALATVNAWAEOI
4 SKKEWLGEDLSEELKKNPFLRELLGWLAEKLPTRSTPTDLILCVPHLYSCLFDRNGDVRKKAQDALPFFMMHLGKMAKATGKLPKTSKDQVLAMLEKAKVNM
5 PAKPAPPTKATSKPMGGSAPAKFQASAPAEDCISSSTEPKPDKKAKAPGLSSKAKSAQGGKMPKSTSLKEDEKSGPIFIVVPNGKEQRMKDEKGLKVLKWNFTTP
6 RDEYIEQLKTMSSCVAKWLQDFMFHSDQHNNKALAVMVDHLESEKEGVIGCLDLILKWLTRFFDTNLSVLMKALEYLKLLFTLSEEEYHLTNEASSFIYLVV
7 KVGEPKDIRKDVRAILNRNCLYYPASKMFFIMEGTGKSNKQRKLEELGCLVESYGMNVQPTFGKALKEIAVHIGLRDNAVRRNAALNTIVTVYVNHGDQVFKL
8 IGNLSEKQDMSMLEERIKRSAKRPSAAPIKQVEEKQORAQNISSNANMLRKGAPEDMSSKLNQARSMSGHPEAAQMVRRREFQLDLEIENDNGTVRCEMPELVQHKLDD
9 IFEPVLIPKIRAVSPHFDDMHQNTASTINFTISQVAVGDINTSIQALTQIDVLRQEDKAEAMSGHIDQFLIATFMQLRLIYNTHMADEKLEKDEITKLYSCLIGN
10 NISLFOEESLAREASTGVLKDLMHGLITLMLDSRIEDEEGGQVRSVNLVVKVLEKSDQTNISALLVLLQDSLLATASSPKFSELVKGLWRMVRLLPDTINSIN
11 LDRILLDIHIFMKVFPKEKPKQCKSEFPIRTLKTLHTLCKLGPKILDHLMIDNKNESELEAHLCRMKHSMDQTGSKDKETEKGASRIDEKSSKAKVNDFLAEI
12 FKKIGSKENTKEGLAELEYKYYKYSADIEPFLKNSQFFQSYVERGLRVIEEMEREGKGRISTSTGIGSPQMEVTCVPTPTSTVSSIGNTNGEEVGPVYLERLKIIRQ
13 RCGLDNTKQDDRPPLTSLLSKPAVPTVASSTDMLSKLSQLRESREHQHSDLDSNGTHSSGTVTSSSSTANIDDLKKRLERIKSSRK

13 A-helix with P: 20/32
14 B-helix with P: 5/27

15
16
17 **GCN1L1** (2671 aa) 61-64 HEAT repeats
18 MAADTQVSETLKRFAGKVTTASVKERRERILSELGKCVAGDLPFEGAVKGLCKLFCLTLRYRDAASRRALQAAIQQLAEQPEATAKLLHSLQSSGKAGVSKS
19 SGSAALLALTWTCLLVRIVFPSPRAKRQGDINWKLVEVQCILLLEVLGGSHKHAVDGAVKKLTWKENPGLVQYLSAILSEPNQNYAGMLGLLVQFCTSHKEMDVV
20 SQHKSALLDFYMKNILMSKVKPPKYLIDSCAPLLRYSLSSEFKLILPTIQSLLRSPENVIEITISSLLASVTLDSQYAMDIVKGLAGHLKNSPRLMDEAVLALRN
21 LARQCSASSANESLTKHLFAILGGSEGLKTVVAQKMSVLSGIVSVSHVVSVPSSQVLNGIVAFIFLPLQQEVHEGTLVHAVSVLALWCRFTMEVPKKLTWFKKA
22 FSLKTSFSAVRHAYLQCMASYGDTLLQALDLLPLLIQTVEKAAQSFOVPTIEGVAALLLLKLSVADSQAFAKLSFFWQLIVDEKQOVFTSEKFLVMASEDALC
23 VVHLHTERLFLDHPHRLTGKVVQYHRAVALVLLSRTHVRRQAQOTVRKLLSSLGGFKLAHGLLEKTVLSSHKVLPLEALVTDAGVTEAGKAYVPPVLOEALC
24 VTSVGPVGLKGDVDTFQLAGFMLIISHPSYAVQSGIWPALLARKIDPEAFITRHLQIIPRMTTQSPNQSSMAMGSLSVLSPDRVLPQLISTITASVQNALR
25 LVTREEFAIMQIPACELDKSITQSAQQDSIKKANMKRENKAYSFKEQIIELELKEEIKKKKGKEEVQLTSKQKEMLQALQDREAAQVRRRLQELDGELEAALGLLDI
26 ILLAKNPSGLTQYIPVLDVDFLPLKSPLAAPRKNPFLSLAACVMP SRLKALGTLVSHVTRLLKPEQVLDXSWQEEELSVAVKRAVMLLHTHTITSRVKGEPGAAP
27 LSAPAFSLVFPFLKMLVTEMPPHSEEEEEWMAQILQILTVQAQLRASPNTPPGRVDENGPELLPRVAMRLTWVIGTGSFRLQVLSADTLTTLCASSSGDGGCAFAE
28 QEEVDVLLCALQSPCASVPETVLRGLNELHMVLPAPDDEKGNLNLRLWVVKFDEEERKLAERLWSMMGLDQPDGSLIDDVYHEAAVRQAGAFALSOAVA
29 RYQFOAAEVMGRLEIYQEKLYPPPVLDALGRVISESPQWENRGLLALNLKLSOYLDSSQVKPLFQFFVDDALNRHPDRKCMDDAALATLNTHGKENVNSLL
30 PVFEEFLKNAPNDASYDAVRQSVVVMGSLARHLDKSDPKVKTIVAKLIAALSTPSQQVQESVAVSCLPPLVPATKEDAGGMTQRLMQQLLES DKYAEKGAAYGLAGL
31 VKGLGILSLKQEMMAALTDAIQKKNFRREGALFAPENLCTMLGKLEPYVHVHLPHLLCFDGNQYVREAADCAKAVMSNLSAHGVKLVLP SLLAALFEESWR
32 KAGSYELLGAMAYCAPKQLSSCLPNIVPKLTVELTDSHVKVKAGQOALRQIGSVIRNPEILATAVLLDALDPSRKTQKCLQTLDTKVFVHIDAPSLALIMPV
33 QRAFQRSTDIRKMAAQIIGNMYSLDQKDLAPYLP SVTPGLKASLLDPVPEVRTVSAKALGAMVKGMGESCFEDLLPWLNETLTYEQSSVDRSGAAQGLAEVMAGLG
34 VEKLEKLMPEIVATASKVDIAPHVRDGYIMMFNYLPIFGDKTPYVGFIIICILKALADENEVRDALTARAGQVISMAYETAIALLLPQLQGLFDLWRIRFSSV
35 QLLGDLDFHTISGVTGKMTTETASEDDNFGTAGSNKAIITALGVERRNRVLAGLYMGRSDTQLVVRDASLHVVKIVVSNTPRTREILPTLFGLLGFLASTGADKRI
36 AARTLGDVRKLGEXILPEIIPILFEGLRSQKSEDEGGVCTGLSETNKSTSDAVLYFSLSLVPTARKALCPLLEEVEAAAKTFEQLHSTIGHQALFDILPFLKQL
37 DDEEVSEFALDGLKQVMAKSRVVLVYLVKLTTPVNTRVLAFLSSVAGDALT RHLGVILPAVLMALKEKLGTPDEQLEMANQOAVILSVEDDTGHRITIEYLLFAT
38 KSPFVGNRQAAAAILNIYCSRSKADYTSHLRSLVSLIRLFNDSPPVLEESWDALNATIKKLDGNGQALIEELHKEIRLIGNESKGEHVPGFCKPKKGVTSILPVL
39 REGVL TGSPEQKEEAALGLVIRLTSADALRPSVVSITGFLIRILGDRFVSNVKAALLETLSLLAKVGIALKPFLLQQTTFKALQDSNRGVRLKAADALGLTS
40 THIKVDPLFTLLNGIRAMEDPGRDMLQALRFVIOGAGAKVDVAVIRKNIIVSLLSMLGHDEDNTRISSAGLGECAFLT EEELSAVLQQCLLADVSGIDWVVRHG
41 RSLALSVAVNVA PGRLCAGRYSSVQEMILSSATADRIPIAVSGVIRMGFLRHHIETGGGLPAKLSSLFVKCLONPSSDRJLVAEKIIWWANKDPLPLDPAIKP
42 ILLKALLQNTKQKNTVIRAYSDDQAVNLLKVRQGEVVFQSLSKILDVASLEVLNEVNRSLKKLASQADSTEQVDDTILT

43 A-helix with P: 39/61
44 B-helix with P: 18/61

45
46
47
48
49
50
51
52
53
54
55
56
57
58
59
60
61
62
63
64
65

Supplemental references

1
2
3 Bednenko, J., Cingolani, G., and Gerace, L. (2003). Importin beta contains a COOH-terminal
4 nucleoporin binding region important for nuclear transport. *J. Cell Biol.* *162*, 391-401.
5
6

7
8 Erickson, H.P. (2009). Size and shape of protein molecules at the nanometer level determined by
9 sedimentation, gel filtration, and electron microscopy. *Biol. Proced. Online* *11*, 32-51.
10
11
12
13
14
15
16
17
18
19
20
21
22
23
24
25
26
27
28
29
30
31
32
33
34
35
36
37
38
39
40
41
42
43
44
45
46
47
48
49
50
51
52
53
54
55
56
57
58
59
60
61
62
63
64
65